This is a repository copy of *Temporal variability in gas emissions at Bagana volcano revealed by aerial, ground, and satellite observations*.

White Rose Research Online URL for this paper:
https://eprints.whiterose.ac.uk/200352/

Version: Published Version

Correspondence to:

B. T. McCormick Kilbride,
brendan.mccormickkilbride@manchester.ac.uk

Temporal Variability in Gas Emissions at Bagana Volcano Revealed by Aerial, Ground, and Satellite Observations

B. T. McCormick Kilbride[1,2] ⓘ, E. J. Nicholson[3], K. T. Wood[4] ⓘ, T. C. Wilkes[5] ⓘ, C. I. Schipper[6], K. Mulina[7], I. Itikarai[7], T. Richardson[8] ⓘ, C. Werner[9], C. S. L. Hayer[1], B. Esse[1], M. Burton[1] ⓘ, T. D. Pering[5] ⓘ, A. J. S. McGonigle[5] ⓘ, D. Coppola[10] ⓘ, M. Bitetto[11] ⓘ, G. Giudice[12] ⓘ, and A. Aiuppa[11] ⓘ

[1]Department of Earth and Environmental Sciences, The University of Manchester, Manchester, UK, [2]Centre for Crisis Studies and Mitigation, The University of Manchester, Manchester, UK, [3]Department of Earth Sciences, University College London, London, UK, [4]Department of Mechanical, Aerospace & Civil Engineering, The University of Manchester, Manchester, UK, [5]Department of Geography, University of Sheffield, Sheffield, UK, [6]Department of Earth Sciences, Victoria University of Wellington, Wellington, New Zealand, [7]Rabaul Volcanological Observatory, Rabaul, Papua New Guinea, [8]Department of Aerospace Engineering, University of Bristol, Bristol, UK, [9]U.S. Geological Survey (contractor), New Plymouth, New Zealand, [10]Dipartimento di Scienze della Terra, Università di Torino, Torino, Italy, [11]Dipartimento di Scienze della Terra e del Mare, Università di Palermo, Palermo, Italy, [12]Instituto Nazionale di Geofisica e Vulcanologia, Catania, Italy

Abstract Bagana is a remote, highly active volcano, located on Bougainville Island in southeastern Papua New Guinea. The volcano has exhibited sustained and prodigious sulfur dioxide gas emissions in recent decades, accompanied by frequent episodes of lava extrusion. The remote location of Bagana and its persistent activity have made it a valuable case study for satellite observations of active volcanism. This remoteness has also left many features of Bagana relatively unexplored. Here, we present the first measurements of volcanic gas composition, achieved by unoccupied aerial system (UAS) flights through the volcano's summit plume, and a payload comprising a miniaturized MultiGAS. We combine our measurements of the molar CO_2/SO_2 ratio in the plume with coincident remote sensing measurements (ground- and satellite-based) of SO_2 emission rate to compute the first estimate of CO_2 flux at Bagana. We report low SO_2 and CO_2 fluxes at Bagana from our fieldwork in September 2019, $\sim320 \pm 76$ td^{-1} and $\sim320 \pm 84$ td^{-1}, respectively, which we attribute to the volcano's low level of activity at the time of our visit. We use satellite observations to demonstrate that Bagana's activity and emissions behavior are highly variable and advance the argument that such variability is likely an inherent feature of many volcanoes worldwide and yet is inadequately captured by our extant volcanic gas inventories, which are often biased to sporadic measurements. We argue that there is great value in the use of UAS combined with MultiGAS-type instruments for remote monitoring of gas emissions from other inaccessible volcanoes.

Plain Language Summary Bagana is a remote and highly active volcano in southeastern Papua New Guinea (PNG). Historically, it has been among the most active volcanoes in PNG, notable for its long-lived eruptions and sustained gas emissions. Bagana has only been infrequently studied before now. We use unoccupied aerial systems (drones) along with ground- and satellite-based remote sensing data to characterize the chemical composition and flux of Bagana's gas emissions and place these in the context of global volcanic emissions. Owing to low activity during the time of our fieldwork, we report lower than anticipated emissions of carbon dioxide and sulfur dioxide from Bagana. We argue that characterizing highly variable volcanic emissions is challenging without long-term continuous observations and that, for remote volcanoes like Bagana, both drones and satellite observations are powerful tools to undertake these observations.

1. Introduction

Bagana volcano, located on Bougainville Island in southeastern Papua New Guinea (6.137°S, 155.196°E; 1,855 m a.s.l.), is among the most active volcanoes on Earth with a record of semi-continuous lava extrusion stretching back to at least the mid-nineteenth century (Bultitude, 1976). Bagana may also be one of the youngest of Earth's active volcanoes; recent estimates suggest that the modern edifice may have grown in only 300–500 years (Wadge et al., 2018). Satellite observations over the past two decades indicate that Bagana is a prodigious source of sulfur

Funding acquisition: B. T. McCormick Kilbride, E. J. Nicholson, I. Itikarai, T. Richardson, M. Burton, A. Aiuppa
Investigation: B. T. McCormick Kilbride, E. J. Nicholson, K. T. Wood, T. C. Wilkes, C. I. Schipper, K. Mulina, C. Werner, B. Esse, D. Coppola, A. Aiuppa
Methodology: B. T. McCormick Kilbride, E. J. Nicholson, K. T. Wood, T. C. Wilkes, C. I. Schipper, T. Richardson, C. Werner, C. S. L. Hayer, B. Esse, M. Burton, T. D. Pering, A. J. S. McGonigle, D. Coppola, M. Bitetto, G. Giudice, A. Aiuppa
Project Administration: B. T. McCormick Kilbride, K. Mulina, I. Itikarai, T. Richardson, M. Burton, A. Aiuppa
Software: E. J. Nicholson, K. T. Wood, C. Werner, C. S. L. Hayer, B. Esse, M. Burton, T. D. Pering, A. J. S. McGonigle, D. Coppola, M. Bitetto, G. Giudice, A. Aiuppa
Visualization: B. T. McCormick Kilbride, E. J. Nicholson, C. Werner, C. S. L. Hayer, B. Esse
Writing – original draft: B. T. McCormick Kilbride, T. C. Wilkes, C. S. L. Hayer, D. Coppola
Writing – review & editing: B. T. McCormick Kilbride, E. J. Nicholson, T. C. Wilkes, C. I. Schipper, K. Mulina, I. Itikarai, T. Richardson, C. Werner, C. S. L. Hayer, T. D. Pering, A. J. S. McGonigle, D. Coppola, M. Bitetto, G. Giudice, A. Aiuppa

dioxide (SO_2) gas into the atmosphere, with a mean annual emission rate of $1{,}379 \pm 89$ kt yr^{-1} during 2005–2015 (Carn et al., 2017). Bagana has been predicted to be a major emitter of volcanic carbon into the atmosphere (~6,245 t d^{-1}), based on global correlations between whole-rock Ba/La ratios and volcanic gas plume CO_2/S_T ratios (Aiuppa et al., 2019; Werner et al., 2019), but the chemical composition of Bagana's gas emissions has never before been measured directly.

The Bagana edifice is steep and unstable, and prone to rockfalls and debris avalanches (Bultitude, 1976). The volcano cannot be climbed safely to deploy gas sensors directly in the plume (cf. Aiuppa et al., 2005; de Moor et al., 2017). Recently, unoccupied aerial systems (UAS, or drones) have been used by volcanologists seeking to measure or sample gas emissions from remote or hazardous summits (James et al., 2020; Kazahaya et al., 2019; Liu, Aiuppa, et al., 2020; Liu et al., 2019; McGonigle et al., 2008; Pering et al., 2020; Rudiger et al., 2018; Stix et al., 2018). Herein, we present the first measurements of volcanic gas chemistry at Bagana, achieved by flying a miniaturized gas sensing payload through Bagana's summit gas plume on-board a UAS. We also present simultaneously acquired remote sensing measurements of SO_2 emission rate. We calculate CO_2 emission rates by multiplying MultiGAS-measured CO_2/SO_2 ratios by these SO_2 emission rates (de Moor et al., 2017; Werner et al., 2019).

Bagana's SO_2 emissions during our fieldwork (13–20 September 2019) were lower than the emission rates calculated from satellite observations in 2005–2017 (McCormick Kilbride et al., 2019). Consequently, our calculated CO_2 emission rates for Bagana are rather lower than those predicted (Aiuppa et al., 2019). We evaluate these results in the context of changeable levels of activity at Bagana, as evidenced by multi-year satellite-based TROPOMI measurements of SO_2 emissions, and the possibility of shallow (i.e., hydrothermal) influences on volcanic gas emissions.

Our results support the developing paradigm that many, and perhaps most, of Earth's volcanoes exhibit wide variations in their gas emissions through time, which can hamper our ability to build volcanic emissions inventories based on short-duration field campaigns or assumptions regarding characteristic activity informed by historical trends (de Moor et al., 2017; McCormick et al., 2015; Werner et al., 2019). Remote volcanoes such as Bagana pose a challenge for the establishment of conventional monitoring networks, and therefore both UAS- and satellite-based methods will be valuable tools for characterizing emissions in such settings.

2. Data and Methods

The key methods used in this study are remote sensing measurements (ground-based UV camera, UAS- and boat-based DOAS spectrometer traverses, satellite-based UV spectroscopy) of SO_2 flux and UAS-enabled in-plume measurements of volcanic gas composition (CO_2/SO_2 molar ratio), using a MultiGAS sensor. CO_2 flux is computed from the product of SO_2 flux and CO_2/SO_2 mass ratio.

2.1. Geological Context

Bagana is one of the seventeen post-Miocene volcanoes on Bougainville Island (Figure 1; Blake, 1968). This volcanism is a consequence of plate convergence, with the Solomon Sea plate being subducted to the northeast beneath the Pacific plate (Holm et al., 2016). Bagana is a stratovolcano of basaltic andesite composition, sometimes described as a "lava cone," being constructed largely of overlapping lava flows with relatively little pyroclastic material (Bultitude et al., 1978). The lava flows are rubbly with prominent marginal levees and steep fronts strewn with talus and fallen boulders. Block-and-ash flows and lahar deposits cover much of the lower northwestern slopes.

Bagana's characteristic activity comprises the alternation of extrusive eruptions persisting for several months and quiescent intervals dominated by voluminous passive degassing. Comprehensive reviews of Bagana's activity are provided by Bultitude (1976, 1981), Bultitude and Cooke (1981) and, more recently, by Wadge et al. (2018) and McCormick Kilbride et al. (2019). The volume of the Bagana edifice is estimated to be 5.1–9.6 km^3, depending on the (unknown) geometry of the underlying topography (Wadge et al., 2018). If the mean extrusion rate of 1.0 m^3 s^{-1} calculated over the last 70 years is representative, the edifice may have been built in only 300–500 years. Intriguingly, the neighboring pyroclastic shield volcano, Billy Mitchell, experienced a caldera-forming VEI 6 eruption 370 ± 19 years before present. Wadge et al. (2018) speculated that there may be a genetic link between caldera collapse and the cessation of activity at Billy Mitchell and the onset of lava extrusion and edifice construction at Bagana.
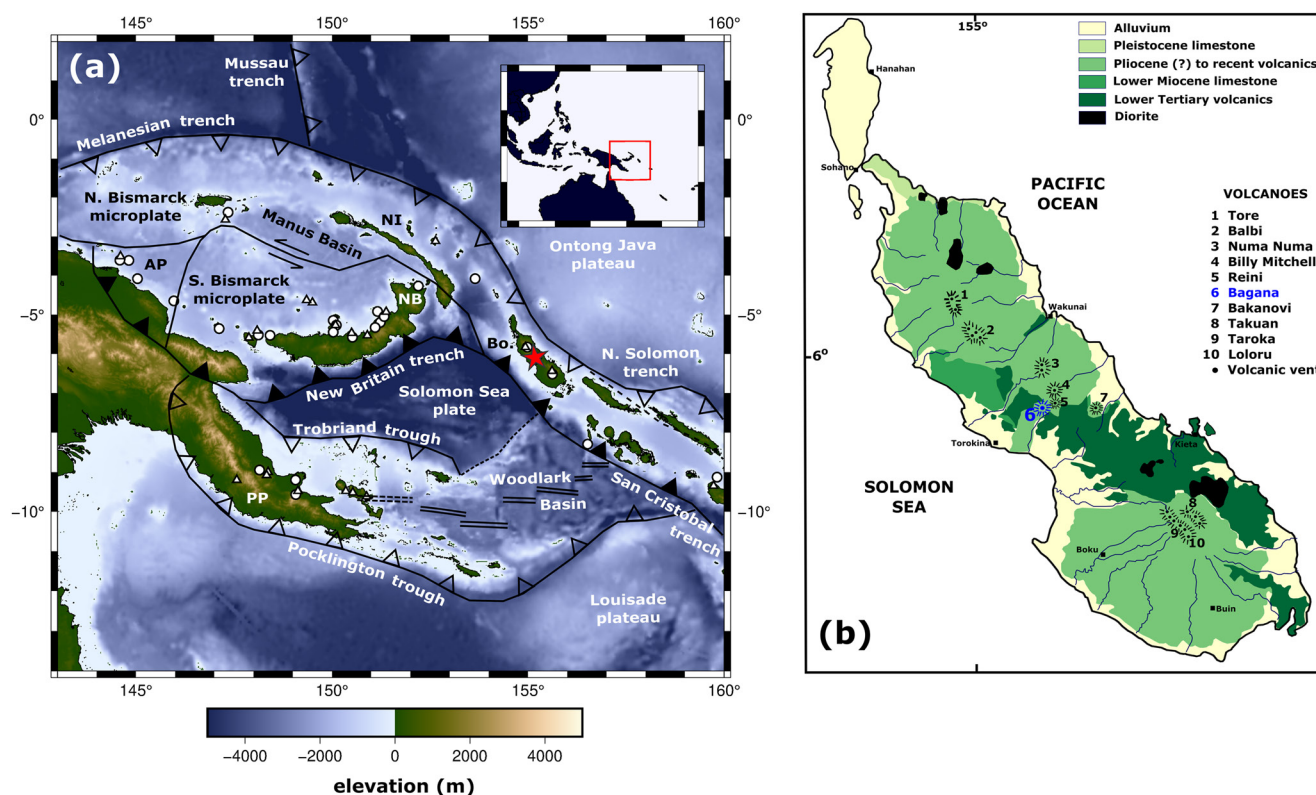
Figure 1. Left panel shows regional geology with key tectonic features marked, after Holm et al. (2016). Bagana is marked with a red star. AP = Adelbert Plate, NB = New Britain, NI = New Ireland, Bo. = Bougainville; PP = Papuan Peninsula. Active plate convergence is marked by black filled triangles; inactive convergent margins are indicated by open triangles. Topography and bathymetry are from the ETOPO1 Global Relief Model (https://www.ngdc.noaa.gov/mgg/global/global.html). Right panel shows Bougainville geological map, with major lithologies and volcanic edifices after Blake (1968).

Measurements of Bagana's gas emissions consistently place it among the largest global volcanic SO_2 sources. Two recent studies used observations from the satellite-based Ozone Monitoring Instrument (OMI). Carn et al. (2017) reported a mean SO_2 flux of 1,380 kt yr^{-1} (3,780 t d^{-1}) in 2005–2015. McCormick Kilbride et al. (2019) distinguished mean co-extrusive and quiescent SO_2 emission rates of 3,300 and 2,500 t d^{-1} respectively, in 2005–2017. Ground-based and airborne UV remote sensing measurements in the 1980s and 2000s found SO_2 emissions in the range of 2,000–3,200 t d^{-1} (Andres & Kasgnoc, 1998; McGonigle et al., 2004). While no measurements have been made of CO_2 emissions from Bagana, Aiuppa et al. (2019) predicted a flux of 6,245 ± 2,335 td^{-1}, based on the combination of Carn et al. (2017)'s reported SO_2 flux and an assumed CO_2/S_T of 2.4 ± 0.7. The latter ratio is based on global correlations between whole-rock Ba/La and volcanic gas plume CO_2/S_T, with Bagana posited by Aiuppa et al. (2019) to be a moderately carbon-rich system, with the local mantle wedge volatile budget being augmented by carbon released from sedimentary lithologies on the nearby subducting slab.

Bagana erupts porphyritic basaltic andesite lavas with phenocryst assemblage of augite, plagioclase and amphibole and a mean whole-rock SiO_2 content of 55.5 ± 1.5 wt. % (Bultitude et al., 1978). The volume of lava erupted over the last decade appears to be insufficient to supply all the gas emitted over the same interval, unless the melt sulfur concentration exceeds ~5,000 ppm, or alternatively the prodigious emissions are sourced from a deeper, non-erupted magma (Edmonds et al., 2022; McCormick Kilbride et al., 2019). At present, there are no petrological or geochemical data to place constraint on the volatile content of the magmas feeding Bagana's eruptions.

2.2. UAS Gas Composition Flights

2.2.1. Titan

Our principal UAS is a fixed-wing aircraft, custom-built at the University of Bristol and based on the twin-propeller V-tail "Titan" airframe from Skywalker (China). We used the Titan aircraft to make the first measurements of
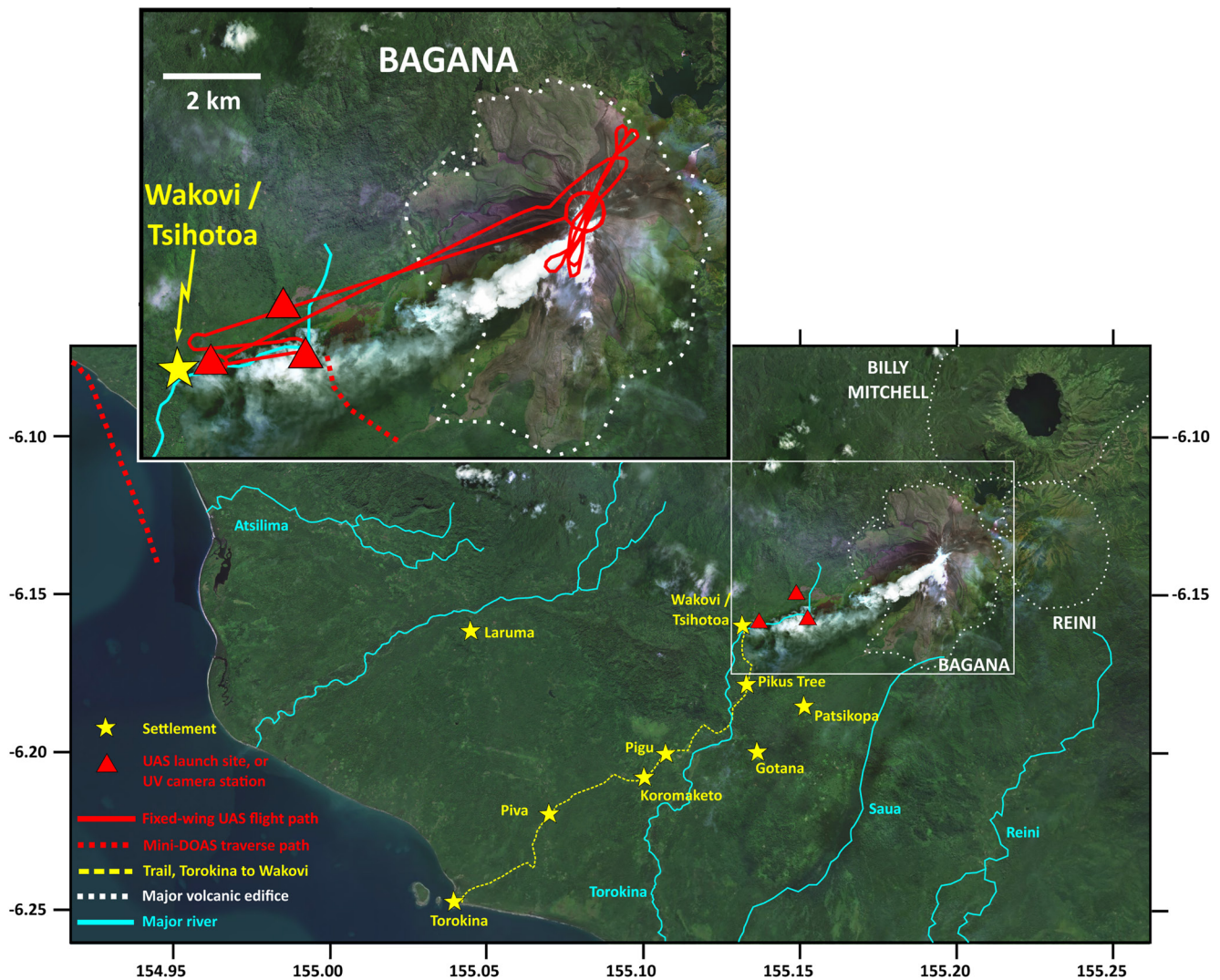
Figure 2. Satellite image (courtesy Bing Imagery) of Bagana surroundings with key locations identified from our fieldwork. We have omitted the flight paths shown in the inset from the main panel for clarity. Adjacent to Bagana are two dormant volcanoes, the pyroclastic shield Billy Mitchell with its summit crater lake and the deeply incised edifice Reini, probably of Pleistocene age. The representative fixed-wing UAS flight path shown corresponds to Flight 6. Paruata Island (Figure 4) is visible offshore from Torokina. Note that the plume shown here is characteristic of Bagana's emissions, which disperse generally toward the southwest, but this image was not acquired during our work in September 2019.

gas composition at Manam volcano, also in Papua New Guinea, and for full details of the UAS configuration we refer the reader to Liu, Aiuppa, et al. (2020) and Wood et al. (2020). Bagana represents a comparable target to Manam in terms of the required endurance (20–25 min flights, with gas sensing measurements undertaken around 2,000 m above take-off altitude and up to 7 km horizontal distance from take-off location).

We launched and recovered the Titan from the hamlet of Tsihokoa (6.159°S, 155.137°E, 150 m a.s.l.) in the Wakovi community, a small ridge above the Torokina river to the west of Bagana (Figure 2). We selected this site because it afforded a clear view of the volcano and plume, had a large open field available for our landing site, and enabled straightforward hand launch of the aircraft into the prevailing wind. To intercept the Bagana plume, we programmed automated flight paths with an altitude gain of 1,700–2,000 m and horizontal traverses of 7 km. We obtained permission for these beyond visual line of sight (BVLOS) flight operations from the Civil Aviation Safety Authority of Papua New Guinea. Our pre-programmed flight paths (example in Figure 2, full series available as a .kml file in Data Set S3) comprised a sequence of waypoints between take-off, a zig-zag ascent path (with optimized ascent rate, climb angle, airspeed etc. chosen based on our experience from previous campaigns), gas sensing over the volcanic summit, a glide back to the recovery area, and a loiter pattern for the aircraft to

maintain until we could safely execute a manual landing. We developed our flight paths iteratively, combining a high-resolution topography model with our own observations of the volcanic summit and plume, both from the ground and from the FPV video stream. We made in-flight adjustments (switching to Fly-By-Wire mode) where necessary, based on real-time readouts from the on-board SO_2 gas sensor. This capability is valuable in that it allows a pilot to change mission targets during flight and also respond quickly to in-flight hazards.

2.2.2. MultiGAS

The Titan carries a miniaturized MultiGAS sensor package in a fuselage payload bay. Our MultiGAS was built at the University of Palermo and is of the same configuration to to those described in Liu et al. (2019), Pering et al. (2020), and Liu, Aiuppa, et al. (2020). Air or gases are pumped (1 L/min flow rate) through a 1-μm particle filter to the sensors and data are logged at 1 Hz. We use SO_2 and H_2S electrochemical sensors (City Technology T3ST/F-TD2G-1A and T3H-TC4E-1A, respectively), calibrated for 0–200 and 0–50 ppmv, respectively, with accuracy of $\pm 2\%$ and resolution of 0.1 ppmv. There is a 13% SO_2 cross-sensitivity on the H_2S sensors and, as described below, we did not detect H_2S in the Bagana plume. We measure CO_2 concentration using a non-dispersive infrared spectrometer (Microsensorik Smartgas Modul Premium2), calibrated for 0–5,000 ppmv with accuracy of $\pm 2\%$ and resolution of 1 ppmv. To avoid radio interference from the UAS transmission system, we wrap the CO_2 spectrometer individually, and the whole sensor payload entirely, in brass foil. We calibrated the sensors with standard reference gases at the University of Palermo before and after the expedition and found no evidence for sensor drift. Our on-board Bluedot BME280 sensor (pressure, temperature, humidity) and our backup both malfunctioned due to rain infiltration during transits through clouds, and therefore we cannot calculate H_2O concentration in the gas plume.

Each flight yields a time series of gas concentration for each sensor, which we post-processed using MATLAB® and Ratiocalc software (Tamburello, 2015). CO_2 concentrations were internally compensated for temperature ($\pm 0.2\%$ full span per °C). We did not make any barometric pressure correction in the calculation of CO_2 concentration: our gas ratios are derived from relative changes in concentration and we flew the UAS at constant altitude during the plume interceptions (Flights 4–6) for which we present data. We distinguish volcanogenic (or "excess") CO_2 from atmospheric background, which we define as the mean CO_2 concentration measured during constant altitude flight in SO_2-free air, updating the value for each flight. We measured no H_2S concentrations exceeding the 13% cross-sensitivity of the sensor to SO_2 (determined during calibration with standard reference gases), and we therefore consider H_2S undetected in the Bagana plume.

We account for different sensor response characteristics within the MultiGAS array by applying a Lucy-Richardson deconvolution algorithm to the CO_2 time series (Liu, Aiuppa, et al., 2020; Pering et al., 2020; Wood et al., 2019). The algorithm is initiated using the measured time series and makes use of a sensor model determined empirically from the response of the NDIR to step changes in calibration gas concentration. The sensor model is best described by a windowed integral and is essentially an N-point moving average applied to the "true" input signal: laboratory tests conducted by Wood et al. (2019) identified the CO_2 sensor to average over approximately 15 s, hence $N = 15$. The deconvolution effectively removes the sensor's inherent filtering effect and the processed CO_2 concentration time series shows concentration peaks (i.e., plume intercepts) that are steeper, narrower and marginally greater in amplitude than the measured signal, without changing the integrated area beneath the peak. We calculate CO_2/SO_2 ratios by fitting linear regressions to scatterplots of SO_2 concentration and our deconvolved CO_2 concentrations. The data selected for inclusion in each fitting are those measured by each sensor during "plume intercepts," intervals where both SO_2 and CO_2 sensors record coincident concentration peaks as the UAS passes into, through, and beyond the volcanic gas plume. The horizontal speed of the Titan is ~ 20 ms^{-1} and the duration of our plume intercepts ranges from ~ 30 to 70 s.

2.3. Ground-, UAS-, and Satellite-Based Remote Sensing

We measured SO_2 emission rates in the field using ultraviolet (UV) spectroscopy, with (a) zenith-pointing spectrometers (e.g., Galle et al., 2003; Kern et al., 2012) making traverses beneath the plume and (b) PiCam UV cameras (Wilkes et al., 2016, 2017). Following the field campaign, we studied SO_2 emissions from Bagana over longer intervals using the satellite-based spectrometer TROPOMI (Burton et al., 2021; Queißer et al., 2019; Theys et al., 2019).

2.3.1. Spectrometer Traverse Measurements

We made traverses by mounting spectrometers on both a second UAS and a boat. This UAS (the "Crabcopter," Figure 3) is a multirotor aircraft under development at the Victoria University of Wellington. This expedition was
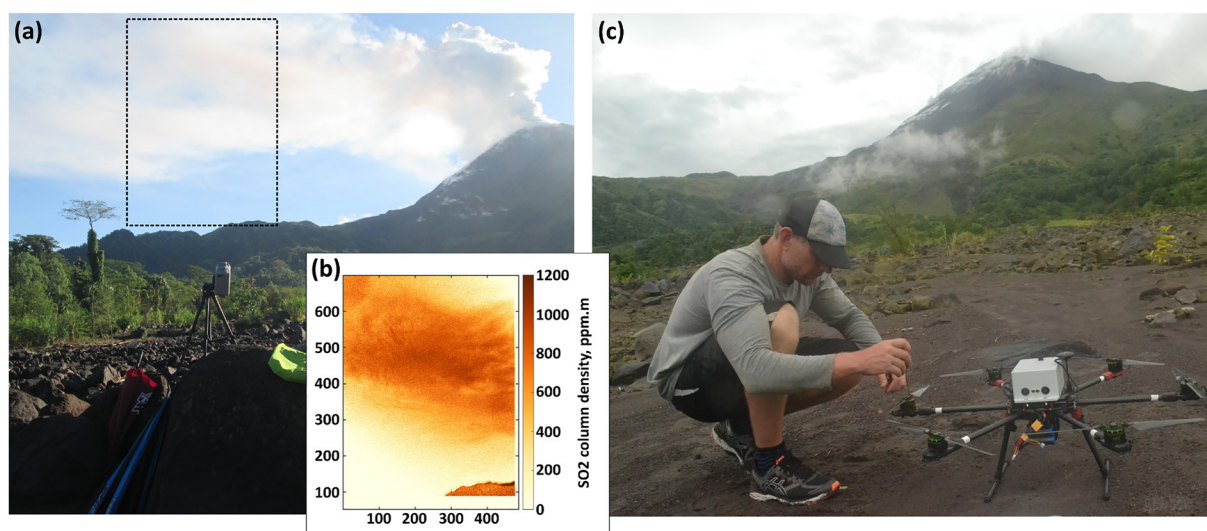
Figure 3. (a) View of Bagana and its gas plume from the UV measurement location (−6.158°S, 155.152°E). Distance to volcano is around 4 km. Dashed box indicates the approximate field of view of the camera while acquiring data. (b) Representative absorption image, with darker colors indicating higher SO$_2$ column density. Ticks and labels on the left and lower edges of the images indicate the scale of the field of view, recorded in meters. (c) Crabcopter pre-flight checks. The miniDOAS spectrometer is housed in the gray box mounted on the upper surface of the UAS.

the first field deployment of the aircraft, which is controlled via wireless link. The operator can view the progress of the aircraft in-flight via a video feed from the on-board action camera, telemetered to a tablet mounted on the ground control unit.

We flew exclusively manual (cf. automated, pre-programmed) flights with the Crabcopter, aiming to make lateral traverses beneath the plume, flying at a steady altitude of 500 m above the ground, from a launch and recovery site at −6.158°S, 155.152°E, around 4 km from the volcano's summit. We were restricted to short observation windows (<1 hr) by persistent cloud cover and achieving a full traverse (i.e., passing from clean air, beneath the plume, and back to clean air) proved challenging due to the large width of the plume (>5 km). During our interval of best (clear-sky) measurement conditions, gas seemed to be ponding around the upper slopes of the edifice, making for large effective plume widths that came close to exceeding the Crabcopter's endurance. Our best traverse, on 17 September, was incomplete and to calculate an emission rate from this measurement, we have had to make an assumption of plume symmetry.

We made further measurements using a spectrometer while leaving the field area by boat on 20th September. We passed beneath Bagana's downwind plume to the southwest (30–40 km from summit, Figure 2); the plume was visible extending a great distance out to sea to our west. At this distance, the plume width was roughly 15 km.

The spectrometer payload is a miniature ultraviolet differential optical absorption spectrometer, or miniDOAS. The instrument quantifies the slant column concentration of a trace gas, here SO$_2$, in its field of view, using scattered sunlight as a light source. The change in light intensity along a known path length due to absorption by SO$_2$, relative to a blue-sky spectrum free of SO$_2$, can be related directly to the SO$_2$ column concentration. Spectral data were acquired between 280 and 500 nm at 0.6 nm resolution and at approximately 1 Hz using an Ocean Optics FLAME-S spectrometer, and the instrument position was tracked using a Ublox NEO-6M GPS receiver. From the vertical column densities obtained in each plume traverse, we can calculate an integrated plume cross section of SO$_2$ concentration. Multiplication of this integrated section by the plume's speed (either from meteorological observations or a model value) provides us with an estimate of SO$_2$ emission rate. Here, we use wind data from GDAS, which is the National Center for Environmental Prediction (NCEP) Global Data Assimilation System (https://www.ncdc.noaa.gov/data-access/model-data/model-datasets/global-data-assimilation-system-gdas). The emission rate error is determined by propagating the errors of the input parameters SO$_2$ column density, wind speed and wind direction by assuming that the individual errors are independent of another. The error in the SO$_2$ column density is determined from the quality of the spectral fit.
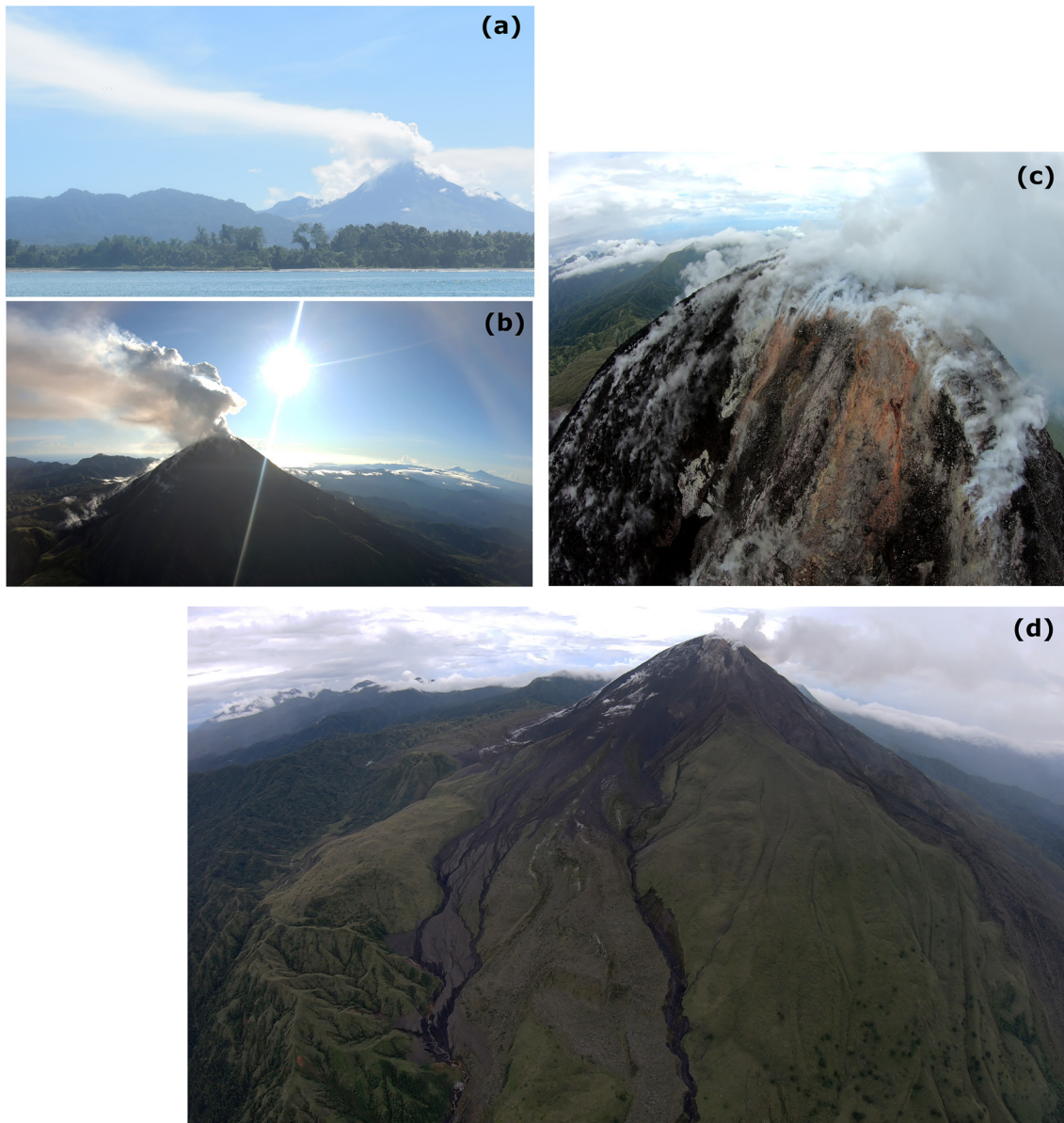
Figure 4. (a) View of Bagana and its large gas plume from Paruata Island on 15 September 2019 (Figure 2), around 22 km southwest of the summit. The steaming 2018 lava flow can be seen descending the left flank of the volcano, abutting against the small dome on the skyline. (b) A northeast-ward view from the Titan's forward-facing action camera, taken during the approach to the volcano in Flight 6. Note the strong vertically rising gas plume and the 2018 lava flow, steaming on the lower left of the image. (c) The summit of the volcano, with extension mineral precipitation and abundant fumaroles. (d) A view from the forward-facing action camera, taken during the approach to the volcano in Flight 4, illustrating the different deposits mantling the edifice. In the lower center of the image is a large braided lava flow with a rubbly surface that erupted in 2010–2012. To the left is a narrow channel of debris avalanche or lahar deposits, which extends several hundred meters further west (behind the aircraft's northeast-ward viewing direction). On the right of the 2010–2012 lava flows is a heavily vegetated suite of lava flows erupted from 1957–1966 (Wadge et al., 2012). At the extreme right of the image are unvegetated rubbly flows mostly erupted in 2000–2005. The lava flows all exhibit prominent channel/levee structures.

2.3.2. UV Camera Measurements

The PiCam is built around two customized Raspberry Pi camera modules (Omnivision OV5647), modified via chemical removal of their Bayer filters to increase responsivity to UV radiation and remove the mosaic pattern response (Wilkes et al., 2016, 2017). The PiCam field-of-view is 23.1° × 17.3° (width × height). Each camera module is equipped with a bandpass filter (Edmund Optics Inc.), one centered at 310 nm and the second at 330 nm (each with 10 nm bandpass full-width-at-half-maximum), which are, respectively, typical on- and off-bands for the detection

of SO_2 (Mori & Burton, 2006). The cameras, Raspberry Pi 3 Model B computers for interfacing, batteries, and a GPS unit are housed in a Pelicase. We manage data capture via custom Python 3 code (Wilkes et al., 2016, 2017).

We carried out image processing after acquisition, not in real-time, and again using custom Python 3 code. Gliß et al. (2017) reviewed SO_2 camera image processing techniques in detail; we primarily use the protocols outlined by Kantzas et al. (2010). Our images are all dark image corrected, and we correct for vignetting using a clear-sky mask acquired in the field. To assess clear-sky background intensity, we measure the average intensity of light in a region of sky close to the plume without volcanic gas. We calibrated our apparent absorbance images using three gas cells of known SO_2 column densities (0, 412, and 1,613 ppm.m). The column densities we measured during the field campaign were all within this calibration range; therefore, we were not required to extrapolate to higher values. We extracted integrated column amounts from a line perpendicular to plume transport (Figure 3) and calculated plume speed with the cross-correlation technique (Mori & Burton, 2006). The prevailing environmental conditions were extremely challenging for UV spectroscopy, with high atmospheric water vapor, persistent cloud cover throughout each day from around 0900 onwards and relatively low UV levels during the early morning and late afternoon clear-sky intervals. Our period of best quality acquisition comprised around 1 hr on the morning of 18 September.

Assuming a 10% uncertainty in our estimated distance from the PiCam to the plume, the estimated distance between integrated column lines for cross-correlation has a corresponding uncertainty of 10%. This translates to a 10% uncertainty in wind speed estimation. We calculated the integrated column amount uncertainty using the PiCam's detection limit of the system, estimated as 180 ppm.m following the method of Kern et al. (2010). Using this as the SO_2 column amount uncertainty and summing in quadrature across each pixel of the integrated column gives an overall integrated column uncertainty (Wilkes et al., 2017). Our measurement geometry, with a vertically spread plume at a relatively close distance, precluded the inclusion of a hillside in our UV images, which precluded the use of Campion et al. (2015)'s image-based correction for light dilution. Given our distance of around 3 km to the plume, we favor a conservative estimate of 20% uncertainty arising from light dilution (Campion et al., 2015). We estimate the cell calibration uncertainty to be 10%, following the manufacturer quoted uncertainty of the gas cell column amounts. Summing all uncertainties in quadrature, our SO_2 camera data are subject to a total uncertainty of 0.7–1.2 kgs^{-1}, or $\approx$25% (Figure 8a).

2.3.3. Satellite Observations

The Tropospheric Monitoring Instrument, TROPOMI, is a hyperspectral imaging spectrometer carried by the European Space Agency (ESA)'s Sentinel-5 Precursor (S-5P) satellite (Veefkind et al., 2012). Launched in 2017 and operational since April 2018, TROPOMI had a spatial resolution of 7×3.5 km^2 (13 times better than the earlier Ozone Monitoring Instrument, OMI), which was improved to 5.5×3.5 km^2 in August 2019. This fine spatial resolution has enabled the mapping of atmospheric SO_2 concentrations with unprecedented detail, in turn enabling the most comprehensive overview yet of volcanic outgassing as observed from space, including monitoring of SO_2 emission rates in both syn- and inter-eruptive episodes at sub-daily temporal resolution (Queißer et al., 2019; Theys et al., 2019).

In this study, we use the COBRA (Covariance-Based Retrieval Algorithm) Level 2 SO_2 TROPOMI data set (https://distributions.aeronomie.be, accessed February 2022; Theys et al., 2021). We calculated SO_2 emission rates from TROPOMI using the PlumeTraj analysis toolkit (Burton et al., 2021; Queißer et al., 2019). The toolkit, written in Python 3, uses the HYSPLIT trajectory model (Draxler & Hess, 1998) to calculate backward trajectories for all pixels in the satellite field of view with confirmed detection of volcanic SO_2. Wind shear within the atmosphere causes trajectories at different altitudes to move at varying speeds and directions; thus, we can isolate those that intersect with the source volcano.

To remove noise from our quantification of SO_2 emission rates, we perform two initial thresholding tests on each pixel: (a) the SO_2 concentration must exceed three times the random noise for that pixel and (b) two of the surrounding eight pixels must also pass this test, removing spurious high concentration pixels. We run all pixels that pass these thresholding tests through the PlumeTraj trajectory analysis. We assign the trajectory that passes closest to the volcano as the optimal trajectory for that pixel, discarding the pixel if the approach distance exceeds 250 km. This optimal trajectory gives us the altitude at the time of measurement, the injection altitude, and the injection time. Since the SO_2 vertical column density (VCD, i.e., concentration) is dependent upon the plume's altitude, raw TROPOMI data are provided assuming three altitudes (1, 7, and 15 km). We use a linear

interpolation between these prescribed altitudes to obtain a corrected concentration for each pixel. We multiply this concentration by the pixel area to give the SO_2 mass which, when combined with the injection time and performed for all pixels in the plume, yields an emission flux time series. We can then average this flux time series to give a daily emission rate, which is reported within this study, along with the peak 1-hr emission rate for each day.

In addition to our PlumeTraj analysis, we calculate monthly mean emission rates (expressed as td^{-1} for each month of the study interval) by regridding and averaging the 1 km COBRA TROPOMI data. Our method follows Theys et al. (2021), using only high-quality pixels (i.e., we discard the outermost 25 pixels from both edges of the swath, those with a cloud fraction >30%, or those with a solar zenith angle >60°) and performing spatial averaging using a 10-point box car average. We stack the regridded data and then divide by the number of positive detections within each grid box. We perform the mass calculation for a 4° box centered on Bagana, with the averaged VCD from each grid box multiplied by its area and then summed. This approach also provides maps of monthly mean SO_2 VCD over the study region (Figure 10, Figure S5 in Supporting Information S1).

We present the satellite time series for two reasons: (a) to affirm an order of magnitude agreement between ground- and space-based observations of Bagana's SO_2 emissions, and (b) to interrogate the long-term trend of emissions since 2017 to the present (i.e., since the analysis of McCormick Kilbride et al. (2019)). Rigorous ground-truthing of the satellite data product is not a key goal of our study due to the limited availability of our ground-based data and the challenging measurement conditions we faced (low UV, short observation windows). Moreover, recent efforts to reconcile ground-based remote sensing measurements with emission rates retrieved from TROPOMI data have already demonstrated the potential for good agreement and robust inter-comparison (Queißer et al., 2019; Theys et al., 2019).

We also show infrared data from the Moderate Resolution Imaging Spectroradiometer (MODIS) instrument, processed using the volcanic hotspot detection system MIROVA developed by Coppola et al. (2016, 2020). MODIS provides data in the mid-infrared (MIR: 3.44–4.13 μm) about four times per day (two at night and two during the day) at a resolution of 1 km. Incandescent material on the Earth's surface (e.g., lava, whether in flows, domes or lakes) is a strong source of thermal energy in the MIR region of the electromagnetic spectrum, a feature which is used by the MIROVA algorithm to detect the presence of sub-pixel hot sources. The level of MIR radiance above that of the surrounding "background" landscape is then used to calculate the Volcanic Radiant Power (VRP), a combined measurement of the area of the volcanic emitter and its effective radiating temperature (Coppola et al., 2016). MODIS data is particularly valuable at Bagana as a direct indicator of active lava extrusion (e.g., McCormick Kilbride et al., 2019; Wadge et al., 2012, 2018).

3. Results

3.1. Volcanic Activity

Bagana was not evidently erupting when we visited in September 2019. Past observations indicate that lava flows are sluggish and that active effusion may be better identified by rockfalls. We observed no incandescence on either summit or flanks and witnessed no ash venting (cf. McCormick Kilbride et al., 2019). The only evidence of recent eruptive activity was a strongly steaming lava flow on the northern flank, which we observed on arrival in the area by boat and from Piva Government Center, our first basecamp (Figures 2 and 4a). Ephemeral steam emissions are common across the edifice, most likely the result of rainwater evaporating. The persistence of the steaming from the northern flank lava flow may indicate some residual magmatic degassing or simply the current hottest point on the volcano's surface. This flow was probably erupted during an interval of sustained thermal anomalies detected by MIROVA satellite observations in July–December 2018 (Global Volcanism Program, 2019a, 2019b, 2019c). Specifically, a short period of effusive activity may have occurred around 6 August 2019, when a peak in radiative power over Bagana was detected by the MODIS satellite and a weak thermal anomaly was observed by Sentinel-2 (Massimetti et al., 2020; https://www.mirovaweb.it/?action=volcanoDetails_S2&volcano_id=255020).

Throughout our fieldwork, we observed sustained, dense white emissions from Bagana's summit, with the plume visibly extending several kilometres over the ocean to the west of Bougainville Island (Figure 4a). From images captured by the Titan's on-board action camera, we saw that the plume is composed of emissions escaping from numerous points on the edifice. There is a dense concentration of fumaroles around the summit and more subdued emissions from the fresh lava flow on the northern flank (Figure 4b; Figure S1 in Supporting Information S1).

Table 1
Summary of Our Seven Gas Sensing Flights With the Titan UAS

Flight	Date, time (GMT+11)	Max SO_2, ppm	Max excess CO_2, ppm	CO_2/SO_2	Error	n[a]	Notes
1	16/09/20, 17:45	–	–	–	–	–	Recon. flight without payload
2	17/09/20, 07:15	–	–	–	–	–	No plume interceptions
3	17/09/20, 08:50	6.2	3.0	–	–	–	Noisy CO_2, did not analyze
4	17/09/20, 13:15	8.1	98.8	5.6	2.9	173	Five plume interceptions
				2.5	8.1		Weighted mean intercepts 1–5
5	18/09/20, 06:45	12.0	72.8	3.2	1.0	468	Nine plume interceptions
		5.9	43.8	4.7	1.5	341	Intercepts 01–06 only
		12.0	72.8	2.9	2.0	127	Intercepts 07–08 only
				4.3	2.2		Weighted mean intercepts 1–9
6	18/09/20, 07:40	12.1	39.9	1.4	0.4	650	Twelve plume interceptions
		7.8	12.1	1.3	0.6	376	Intercepts 01–07 only
		12.1	39.9	1.5	0.6	274	Intercepts 08–12 only
				1.3	0.2		Weighted mean intercepts 1–12
7	18/09/20, 08:45	–	–	–	–	–	Abandoned flight due to rain
4–6[b]	–	12.1	98.8	2.4	0.6	1,311	Linear regression, 4–6
		12.1	98.8	1.6	0.2	1,311	Weighted mean, 4–6
		12.1	98.8	1.4	0.2	674	Weighted mean, 4–6 ($SO_2 > 5$ ppm)
		12.1	98.8	1.6	0.8	196	Weighted mean, 4–6 ($SO_2 > 10$ ppm)

Note. Date and time are in Bougainville local time.

[a]n is the number of measurements (at 1 Hz) used in the calculation of the ratios, effectively equal to the total duration of gas sensor contact with the volcanic plume (in seconds). [b]This line refers to CO_2/SO_2 ratios calculated by incorporating data from Flight 4, Flight 5 and Flight 6.

The majority of the emissions originate from the summit, which is encrusted with white, gray and yellowish mineral deposits (Figure 4c).

Residents of the Wakovi community (Figure 2) reported that no substantial explosive activity has occurred at Bagana since 2014, when hot ashfall ignited house roofs and the community schoolhouse and resulted in temporary self-evacuations to communities near the coast. Villagers reported a number of lines of evidence by which they infer imminent eruptions including vegetation dieback along the upper reaches of the Torokina River due to rising water temperature, presumably a result of heat transfer from rising magmas. The principal risk to the local community results from debris avalanches, including lahars, locally called *tovure*, which pass from the edifice slopes into the upper reaches of the Torokina river. As with our previous visit in 2016, the western approaches to the volcano are covered in thick debris flow deposits, quite distinct from both recent and historic lava flows (Figure 4d).

3.2. Gas Composition

We made seven flights over Bagana's summit with the Titan UAS and encountered the gas plume on Flights 4, 5, and 6. We have described all flights fully in our Supporting Information S1, discussing planned and realized flight paths and describing the plume intercepts in terms of peak gas concentrations and the topology of the gas concentration time series. We also discuss different means of deriving CO_2/SO_2 ratios across each flight, with the resulting ratios all presented in Table 1. In Figure 5, we show the molar CO_2/SO_2 ratio for each plume intercept, grouped by flight, and plot these ratios as a function of plume exposure time and peak SO_2 concentration. In Figure 6, we show the full CO_2 and SO_2 concentration time series measured by our MultiGAS during Flight 6 and the CO_2–SO_2 scatterplots we used to derive CO_2/SO_2 ratios for Flight 4, Flight 5, and Flight 6. In Figure 7, we plot CO_2 and SO_2 concentrations along the Titan flight path during Flight 6. The full time series for Flights 4 and 5 are in Supporting Information S1 (Figure S2) and the gas concentrations along the flight paths for these flights are in Supporting Information S1 (Figure S4).

Figure 5a shows the CO_2/SO_2 ratios we calculate for individual plume intercepts. These vary widely and are subject to large uncertainties due to the low concentrations of gas that the Titan encountered and the short
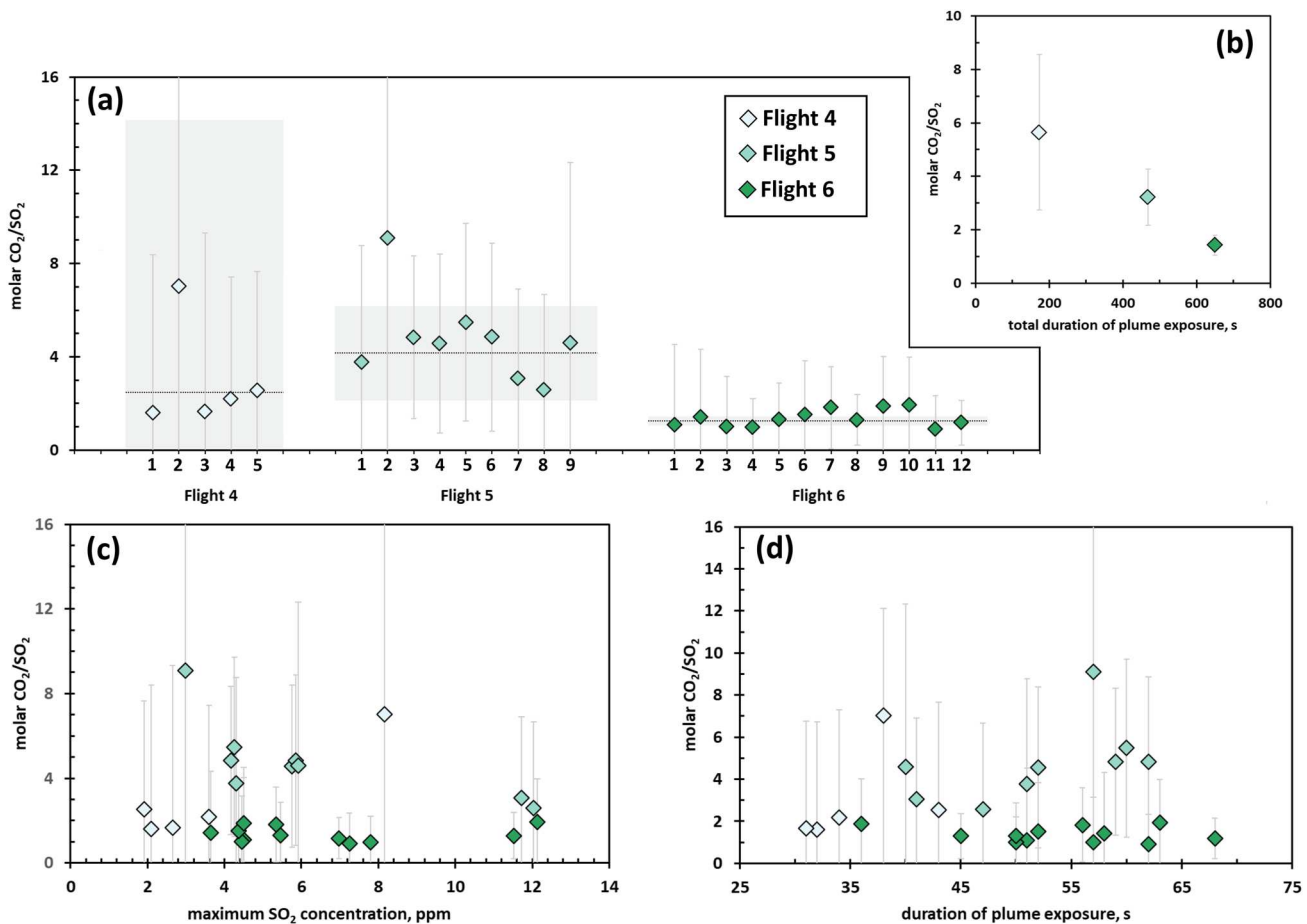
Figure 5. (a) The diamond-shaped data points show molar CO_2/SO_2 ratios obtained for individual plume intercepts, colored according to flight. The dashed horizontal lines show the weighted mean CO_2/SO_2 ratio obtained by averaging the per-intercept ratios, with the weighting factor based on the per-intercept errors (shown by vertical bars on the diamonds). The shaded panels show the errors on these weighted means. (b) Molar CO_2/SO_2 ratios obtained for each flight, calculated from linear regressions between SO_2 and excess CO_2 concentration data from all intercepts (Flight 4, $n = 5$; Flight 5, $n = 9$; Flight 6, $n = 12$). Compared with per-flight weighted mean ratios shown by shaded bars in (a). (c) Molar CO_2/SO_2 ratios obtained for individual plume intercepts, plotted against the corresponding maximum SO_2 concentration (ppm) measured during the intercept. (d) Molar CO_2/SO_2 ratios obtained for individual plume intercepts, plotted against the duration of sensor exposure to the volcanic plume.

duration of sensor exposure to the volcanic plume. We do not see strong correlations between per-intercept CO_2/SO_2 ratios and peak SO_2 concentration (Figure 5c) or exposure time (Figure 5d). In Flight 6, our per-intercept ratios remained relatively stable across a range of SO_2 concentration and time spent in the plume, while Flights 4 and 5 show more internal variability. We do see significantly lower errors on the ratios calculated across each flight as the duration of gas-sensor contact increased (Figure 5b). We see no evidence for systematic spatial variations in plume composition (Figures S3 and S4 in Supporting Information S1). Our measured SO_2 and excess CO_2 concentrations tend to be higher when the UAS was closer to the volcano's summit, but there is no correlation between distance to the summit and instantaneous CO_2/SO_2 molar ratio.

To derive Bagana's CO_2 emission rate (see below), we multiply SO_2 emission rates measured via UV remote sensing by a representative CO_2/SO_2 ratio. The ratio we calculate from our Flight 6 data is subject to lower errors than the Flight 4 and 5 ratios (Table 1) and there is less variation in the per-intercept ratios within Flight 6 (Figure 5a). However, the Titan did unambiguously encounter the volcanic plume several times across Flights 4 and 5. We cannot rule out that the differences in gas composition between each flight are genuinely reflecting spatial or temporal variations in plume chemistry, rather than being consequences of our sampling approach. Therefore, we consider that the overall CO_2/SO_2 ratio should be based on as much of our data from these three successful flights as possible. If we combine Flights 4–6 and fit a single linear regression through the data, we obtain CO_2/SO_2 of 2.4 ± 0.6. Alternatively, we can calculate a weighted mean CO_2/SO_2 ratio of 1.6 ± 0.2 from our ($n = 26$) individual
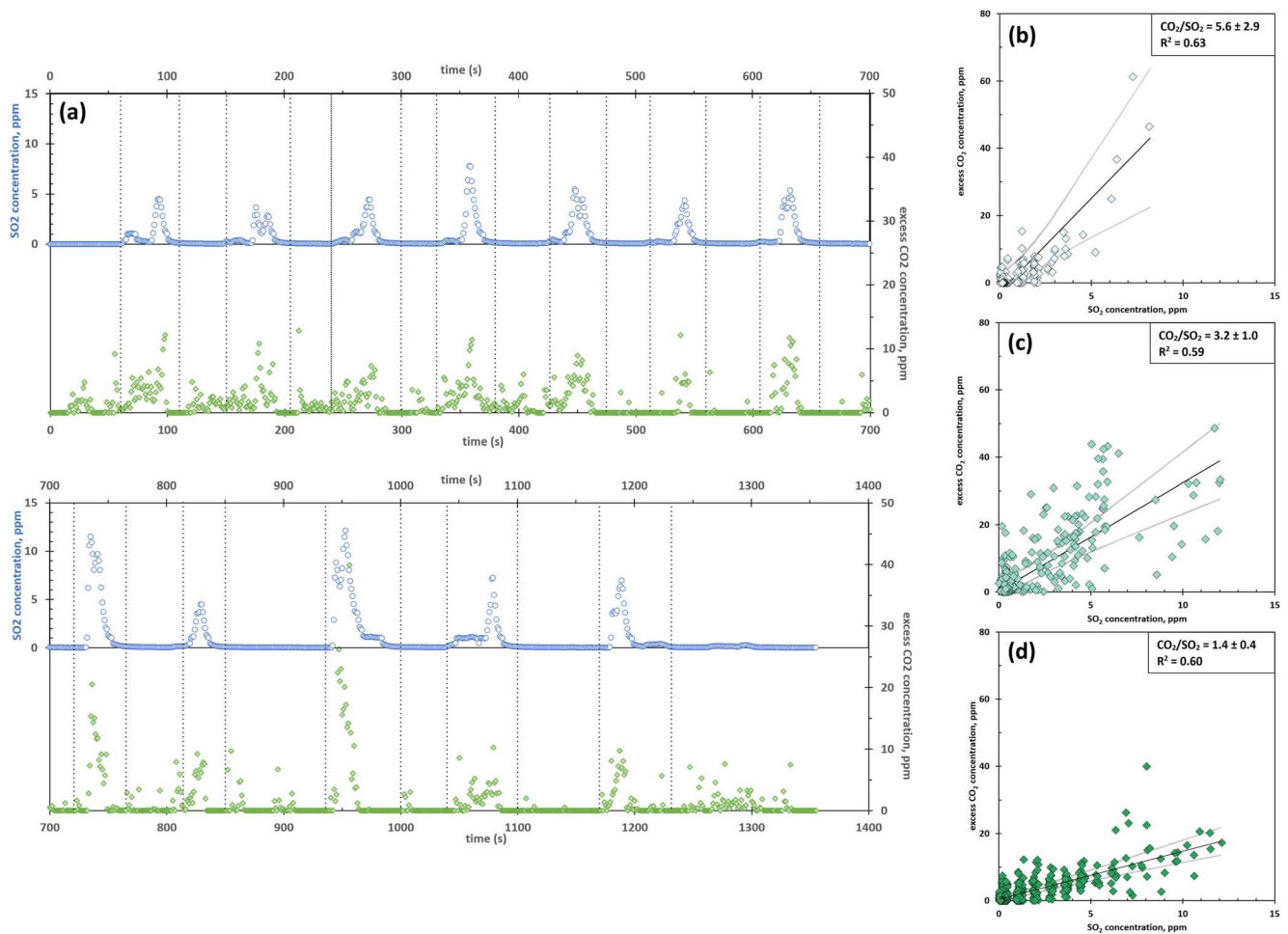
Figure 6. (a) Time series of SO_2 (blue) and excess CO_2 (green) concentrations measured by MultiGAS during intercepts of Bagana's plume during Flight 6, and correlation plots of SO_2 and excess CO_2 concentrations and molar CO_2/SO_2 ratios for (b) Flight 4, (c) Flight 5, and (d) Flight 6. Black lines are the linear regressions from which we derive the ratios; gray lines show the 95% confidence intervals. Vertical gray dashed lines on the time series indicate the "intercept" intervals (SO_2 concentration above the sensor noise) where the UAS flew through the volcanic plume, and which we used to derive per-intercept molar CO_2/SO_2 ratios.

plume intercepts, weighting our calculation according to the error on each intercept, aiming to limit the influence of highest uncertainty data on the overall "representative" ratio. This is to establish mean CO_2/SO_2 only, and not to disregard potential temporal variations in composition between flights. Filtering the data to calculate a ratio from plume intercepts where SO_2 concentration exceeded 5 ppm ($n = 12$) and 10 ppm ($n = 4$), yields molar CO_2/SO_2 of 1.4 ± 0.2 and 1.6 ± 0.8 respectively, that is, without significant change in the ratio but with increase in uncertainty.

3.3. Sulfur Dioxide Emissions

Our most reliable UV camera data comprise around 1 hr of measurements on the morning of 18 September (first acquisition, 0805–0830; second acquisition 0835–0905) (Figure 8a). Despite relatively low UV levels due to the early time of day, clear skies prevailed over the volcano. Measurement attempts on the previous 2 days were thwarted by thick cloud cover, rain showers and weak SO_2 emissions.

We calculate mean ($\pm$standard deviation) SO_2 emission rates of 4.65 ± 0.28 kgs^{-1} (401 ± 24 td^{-1}) in the first acquisition and 3.37 ± 0.37 kgs^{-1} (292 ± 32 td^{-1}) in the second (Figure 8a). The apparent decline in SO_2 flux through the observation period may be a volcanological phenomenon, though we observed no changes in activity, or a consequence of changing light levels influencing the instrument calibration.

We also measured SO_2 emissions using mini-DOAS spectrometer traverses (Figure 8b). When close to the volcano on 17 September, our UAS-mounted spectrometer failed to complete a full traverse of the plume. Despite
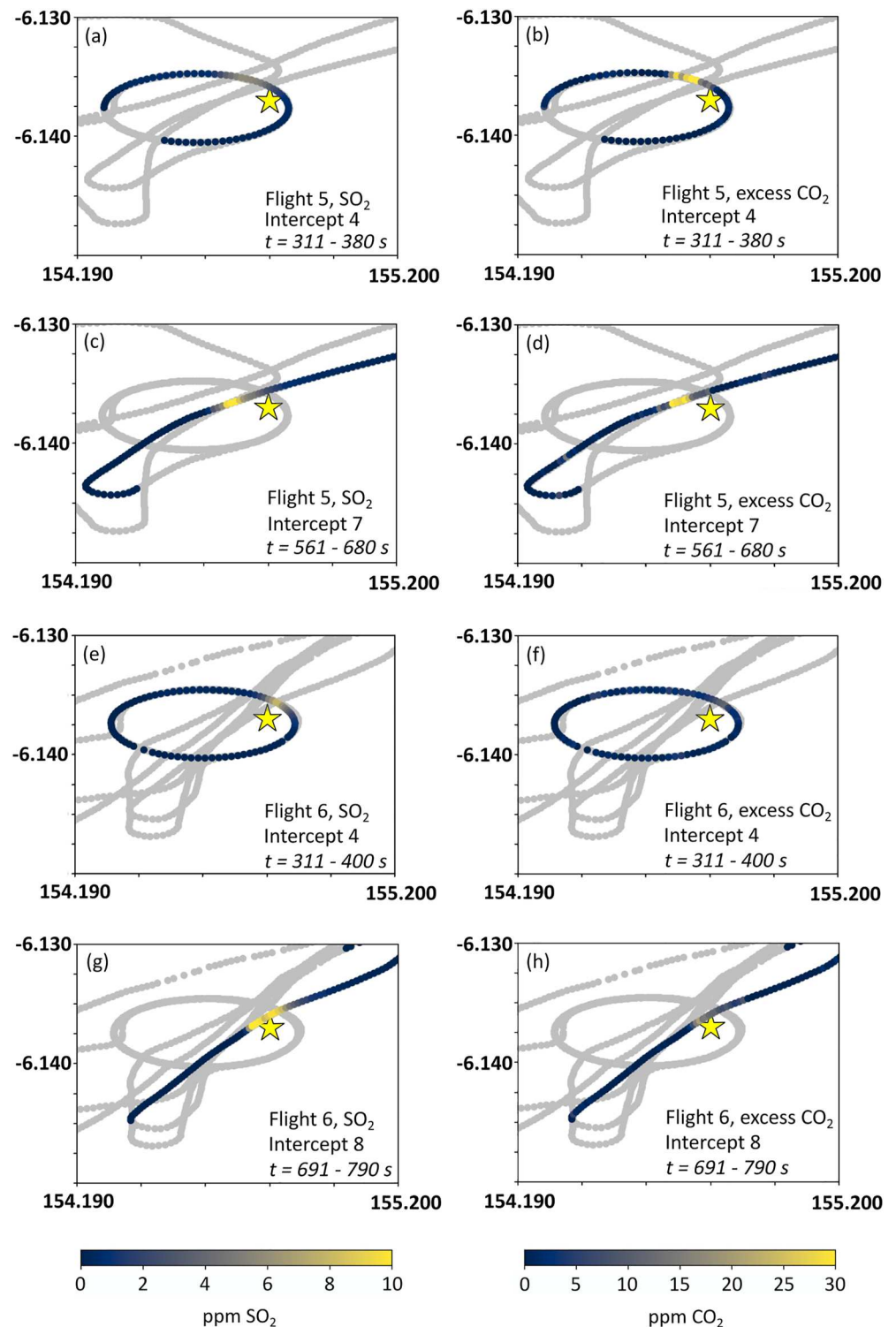
Figure 7. Gas concentrations measured by airborne MultiGAS in Flight 5, intercept 4 (a, b) and intercept 7 (c, d) and Flight 6, intercept 4 (e, f) and intercept 8 (g, h). The gray lines show the full path of each flight; colors illustrate the gas concentration, of SO_2 (a, c, e, g) and excess CO_2 (b, d, f, h). The yellow star represents the volcano's summit. Each map covers the same area; all SO_2 panels and CO_2 panels, respectively, have consistent color scales. The full extent of gas sensing intervals (i.e., plume intercepts) from Flights 4–6 are shown in Supporting Information S1 (Figure S4).
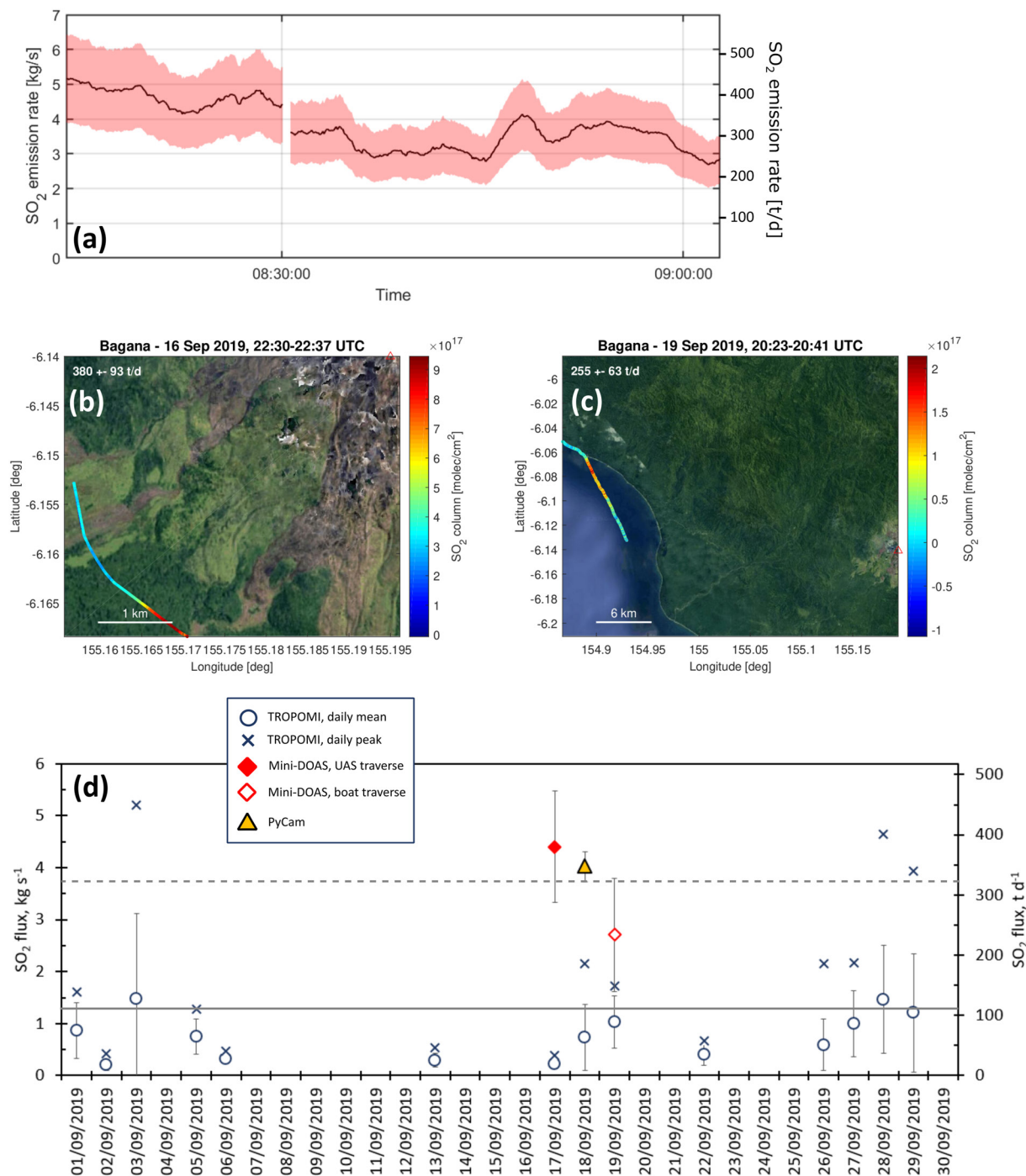
Figure 8. (a) Time series of SO$_2$ flux from UV camera acquisition on the morning of 18th September 2019, with one sigma uncertainty about the calculated flux value; (b) Maps of SO$_2$ vertical column density measured by mini-DOAS in traverses by multi-rotor UAS (left, 17th September 2019) and boat (right, 20th September 2019). (c) Composite daily SO$_2$ emission rate time series through September 2019, incorporating TROPOMI satellite observations and the ground-based remote sensing data we collected during our fieldwork. Horizontal dashed line shows the mean SO$_2$ emission rate from ground-based data; horizontal solid line shows the mean SO$_2$ emission rate from satellite-based data.

this, we can estimate SO$_2$ emissions from a partial traverse at 380 ± 92 td^{-1}. If we assume that we captured the majority of the plume, this value should be within the error of the true emission rate. As we were leaving the field area by boat on 20 September, we made zenith-pointing traverses with two mini-DOAS instruments. The plume was around 15 km wide at this distance ($\sim$35 km) from the volcano summit. The resulting emission rates were 251 ± 122 t/d and 234 ± 94 t/d, thus consistent with one another.
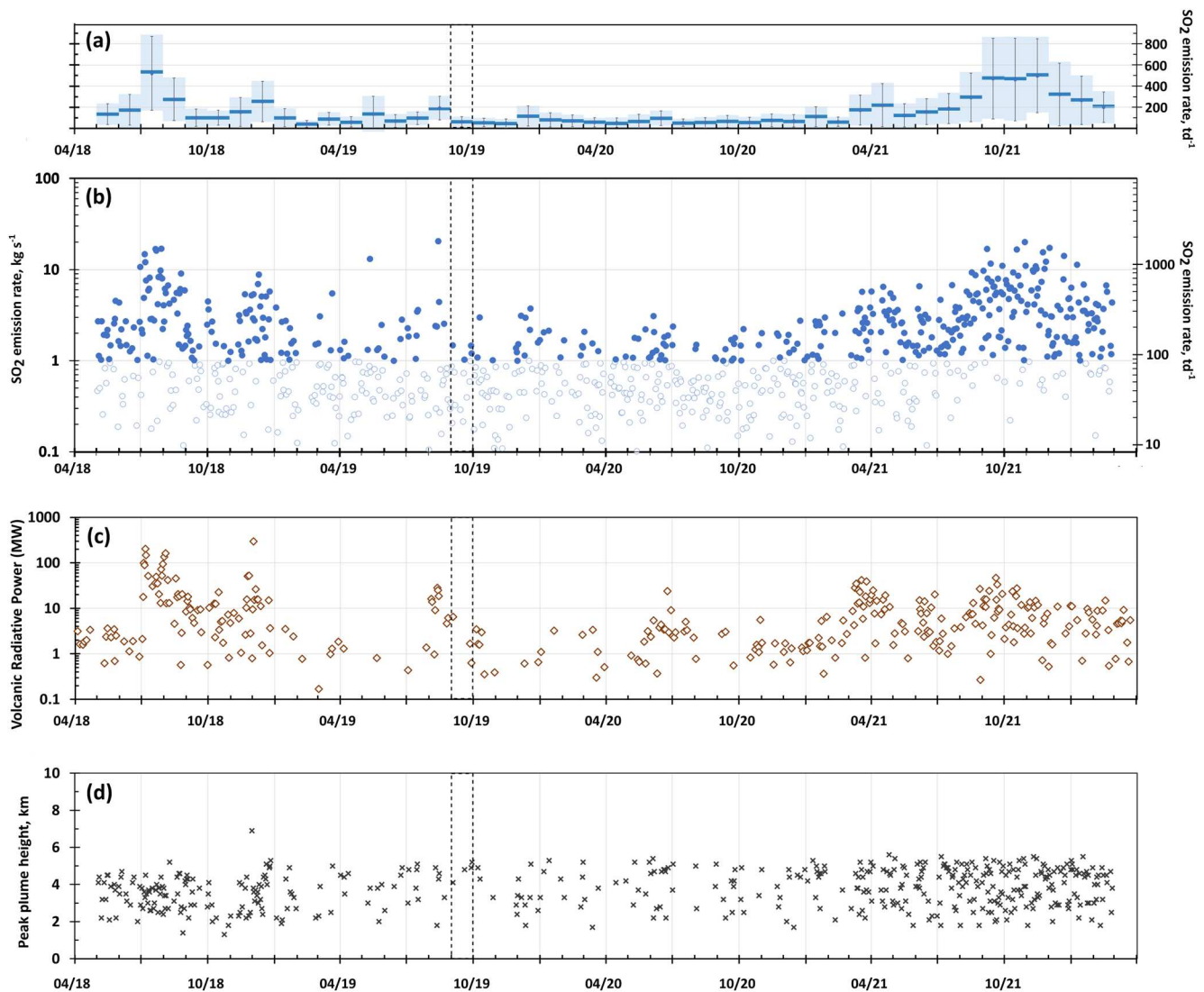
Figure 9. Satellite observations of Bagana's activity from May 2018 to present. (a) Mean (±standard deviation) SO$_2$ emission rate for each month of our study interval, derived from TROPOMI observations; (b) daily mean SO$_2$ emission rates retrieved from TROPOMI observations, with days where flux is below 1.0 kg s^{-1} (~90 td^{-1}) and thus subject to greater uncertainty shown in paler colors; (c) volcanic radiative power, expressed in MW, obtained from the MIROVA system's analysis of MODIS thermal infrared retrievals over Bagana; (d) Maximum plume height retrieved per day, obtained from PlumeTraj analysis of TROPOMI retrievals. In each panel, the vertical black dashed lines highlight September 2019, when our fieldwork took place.

3.4. Satellite Observations of Gas and Thermal Emissions

TROPOMI observations allow us to quantify SO$_2$ emissions from May 2018 to February 2022 (Figures 9 and 10, Figures 5Sa–5Sl in Supporting Information S1). Over this interval, we obtained an estimate of the mean daily SO$_2$ flux on 885 days, of which 453 days saw the mean flux exceed 1.0 kg s^{-1}. TROPOMI failed to detect a plume from Bagana on 505 days, due either to emissions dropping below the sensor's resolution, cloud cover, or none of our PlumeTraj trajectories returning to Bagana. In September 2019, we have 14 days with estimates of SO$_2$ flux, with an average of 0.75 kg s^{-1} (65 td^{-1}) and a maximum peak daily flux of 5.20 kg s^{-1} (450 td^{-1}). Generally, our satellite-based emission rates in September 2019 are lower than those measured by ground-based remote sensing in the field (Figure 8d). We are unable to rigorously evaluate whether this is due to different sensitivities, measurement geometries, or time or duration of measurement (i.e., satellite-based fluxes are constructed over several hours, our ground-based measurements each cover <1 hr). The mean (±S.D.) SO$_2$ emission rate in September 2019 if we combine our satellite and ground-based measurements is 116 ± 118 td^{-1}. This is lower than the mean of the ground-based measurements we made during our fieldwork and may be due to lower activity and emissions
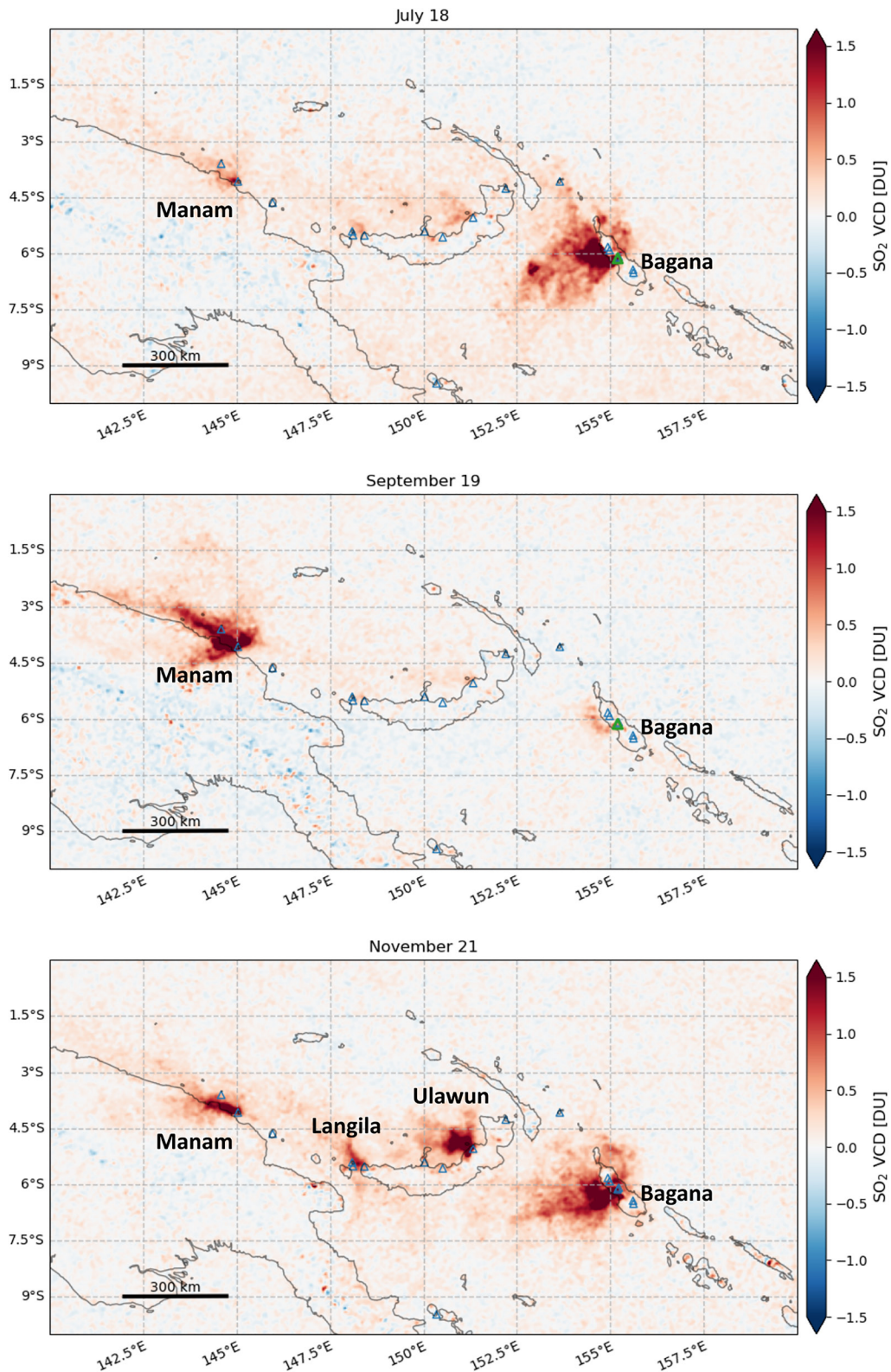
Figure 10. Average atmospheric SO$_2$ vertical column densities over Papua New Guinea, as observed by TROPOMI for July 2018 (top), September 2019 (middle) and November 2021 (bottom). We construct these maps by averaging all TROPOMI observations acquired in each month. In July 2018 and November 2021, Bagana was in a state of active lava extrusion accompanied by elevated SO$_2$ gas emissions. In September 2019, coincident with our field campaign, Bagana was in much lower state of activity (no visible eruption) and reduced gas emissions. Note SO$_2$ emissions of varying strength from other volcanoes across the region: Manam, Langila, and Ulawun.

in the remainder of the month or a low bias resulting from reduced TROPOMI sensitivity during periods of lower emissions (e.g., low altitudes, low vertical column densities).

Our satellite observations suggest three broad phases of contrasting activity at Bagana since 2018: (a) from May to December 2018, SO_2 emissions are relatively high with mean ($\pm$S.D.) daily emissions per month ranging from 100 ± 70 to 520 ± 348 td^{-1}; (b) from January 2019 to March 2021, SO_2 emissions are relatively low with mean daily emissions below 100 td^{-1} in every month except August and December 2019; and (c) since March 2021, SO_2 emissions are relatively high again, with mean daily emissions per month ranging from 123 ± 109 to 498 ± 350 td^{-1} (Figure 9a). The large relative magnitude of the standard deviation to the mean points to high inter-daily variation in SO_2 emission rates (Figure 9b). Independent observations from the MODIS thermal infrared sensor, processed with the MIROVA algorithm (Coppola et al., 2016, 2020), support the notion of three periods of activity, with elevated thermal emissions in May–December 2018 and since March 2021, with an intervening period largely characterized by the absence of thermal emissions (Figure 9c). Peak SO_2 plume heights, another output of our PlumeTraj routine, do not show systematic variations with either SO_2 emission rate or thermal flux, but tend to lie between 2 and 5 km for the entire study interval (Figure 9d).

4. Discussion

4.1. Carbon and Sulfur Fluxes From Bagana, and Implications for Regional Emissions Budgets

The molar CO_2/SO_2 ratio for Bagana's plume is 2.4 ± 0.6 if we calculate it via a single linear regression through all our MultiGAS data from Flights 4–6, or 1.6 ± 0.2 if we calculate it via an error-weighted mean of our 26 per-intercept CO_2/SO_2 ratios. The "combined linear regression ratio" may obscure temporal variation in gas composition between each flight, while the "error-weighted mean ratio" more explicitly accounts for temporal variations. Our error weighting of the mean compensates for the short duration of individual plume intercepts.

Our data ($CO_2/SO_2 = 1.6 \pm 0.2$) suggest Bagana's gas emissions are carbon-poorer than, but overlap within error with, the composition ($CO_2/SO_2 = 2.4 \pm 0.7$) predicted from global relationships between CO_2/SO_2 in high temperature volcanic gas emissions and Ba/La (or Sr/Nd) in erupted rocks (Aiuppa et al., 2019). All Papua New Guinea's volcanoes, including Bagana, were assigned to "Group 2", volcanoes characterized by relatively carbon-rich emissions due to efficient recycling of slab carbon into the sub-arc mantle. Whether this is true for Bagana remains open to debate. There are no direct samples of the subducting slab in the Solomon Sea (e.g., piston cores seaward of the Bougainville trench), just dredges and a free-fall grab from the *R.V. Natsushima*'s 1983–1984 cruise (Crook, 1987; Woodhead et al., 1998). The sampled lithologies comprise volcaniclastic sediments, mudrocks and only minor limestones. It is not clear how well these samples reflect the slab composition at sub-arc depths. Trace element (e.g., Th/Yb vs. Sr/Nd) and radiogenic isotope (i.e., Sr-Nd-Pb) data for lavas from Bagana and other Bougainville volcanoes suggest a fluid-dominated slab flux and only minor sedimentary influence (Hergt et al., 2018). This may explain our relatively carbon-poor gas compositions, but further work is required to characterize volatile provenance in this arc segment.

The gas composition predicted by Aiuppa et al. (2019) is based on the chemistry of lavas erupted over decades (Bultitude et al., 1978). Our data are direct measurements of Bagana's emissions but represent just 2 days of relatively low-level activity for this volcano. Considering this, the fact that the two estimates match within error is perhaps surprising. Volcanoes can exhibit dramatic temporal changes in gas composition, with CO_2/SO_2 increasing following mafic recharge into shallow crustal reservoirs or as unrest builds prior to eruptions (e.g., Aiuppa et al., 2007; Werner et al., 2019). Our data do not allow us to predict whether Bagana's gas composition might vary as a function of activity, but it seems plausible that co-eruptive emissions may differ in composition to the gases we measured in September 2019, a period of relative quiescence. If we consider a general degassing model of andesitic volcanoes (e.g., Edmonds et al., 2022) that sees surface gas emissions as mixtures of deeply exsolved (CO_2-rich) fluids delivered largely through the second boiling of intruded hydrous magmas, and more S-rich fluids released during shallow crystallization or ascent and extrusion, we may interpret our relatively low measured CO_2/SO_2 as the product of residual degassing of shallow-stored magma that ascended to the upper reaches of Bagana's plumbing system but was not erupted. Thus, while our calculation of CO_2 emission rates relies on our measured CO_2/SO_2 ratio, we note that this may not closely resemble Bagana's "true" long-term gas composition.

We measured Bagana's SO_2 emission rate using a combination of a UAS traverse with mini-DOAS, a boat traverse with mini-DOAS, the PiCam, and TROPOMI satellite observations (Figure 8c). The mean ($\pm$standard deviation)

SO_2 emission rate from our ground-based measurements (PiCam and mini-DOAS) is 320 ± 76 td^{-1}. These are the lowest emission rates yet measured at Bagana. Earlier campaign measurements reported SO_2 fluxes of 3,100 td^{-1} in 1983 and 3,200 td^{-1} in 1989, 1,900 td^{-1} in 2003, and 3,900 td^{-1} in 2016 (D'Aleo et al., 2017; Global Volcanism Program, 1983, 1989; McGonigle et al., 2004). Multi-year satellite observations have also suggested typical SO_2 emissions of $\geq 10^3$ td^{-1} from 2005 to 2018 (Carn et al., 2017; McCormick et al., 2012; McCormick Kilbride et al., 2019).

Since 2018, our new satellite observations suggest three intervals of differing behavior, defined above in terms of SO_2 and thermal emissions as (a) May–December 2018; (b) January 2019–March 2021; and (c) March 2021 to present. Our interpretation of these three intervals is that the first and third represent episodes of lava extrusion, while the second is a period of quiescence accompanied by passive SO_2 emissions (Figure 9). Elevated gas emissions accompanying active extrusion, interpreted from a striking correspondence between SO_2 and thermal emissions, seem to be a characteristic feature of Bagana (McCormick Kilbride et al., 2019; Wadge et al., 2018) and is further evident in activity reports compiled by the Smithsonian Global Volcanism Program. The first interval of elevated gas and thermal emissions is likely to have coincided with the extrusion of the fresh lava flow we observed in Bagana's northern flank during our fieldwork in September 2019. In spring 2021, thermal anomalies were detected by the Sentinel-2 satellite, initially confined to the summit area before spreading to the northern flank (Global Volcanism Program, 2021a, 2021b). At the time of writing, we assume this lava extrusion may still be ongoing (https://www.mirovaweb.it/?action=volcanoDetails_S2&volcano_id=255020). Overall, our SO_2 data from September 2019 are consistent with the general decline in activity at Bagana since 2012 (Global Volcanism Program, 2019a, 2019b, 2019c, 2020; McCormick Kilbride et al., 2019). The volcano exhibits a wide range in the intensity of its activity (further borne out by our satellite data in this study, Figures 9 and 10; Figures 5Sa–5Sl in Supporting Information S1) and our field campaign coincided with a period of particularly low-level unrest.

The Bagana edifice is likely to be partly saturated with water, owing to heavy daily rainfall. There are numerous fumaroles on the summit rather than a single "open vent," extensive mineral precipitation around these fumaroles, and faint odors of sulfur in the small rivers around the volcano (Figure 4c). However, we did not detect any H_2S in the Bagana gas plume and therefore consider it unlikely that our SO_2 emission rates are strongly influenced by scrubbing (e.g., Symonds et al., 2001).

A molar CO_2/SO_2 ratio of 1.6 ± 0.2 is equivalent to a mass ratio of 1.1 ± 0.1. Multiplying this by our mean ground-based SO_2 emission rate of 320 ± 76 td^{-1} yields a CO_2 flux of 320 ± 84 td^{-1}. This is our best estimate for Bagana's carbon emissions at the time of measurement in 2019, given the comparable temporal duration of our UAS-based plume composition data and our ground-based SO_2 emission rate data. Considering September 2019 as a whole, and our combined satellite plus ground-based SO_2 emission rate data, we estimate a CO_2 emission rate of 128 ± 130 td^{-1}. This estimate is subject to two key uncertainties, namely the assumption of fixed CO_2/SO_2 throughout the month, and whether the ground- and satellite-based estimates of SO_2 emissions can be seamlessly combined. The potential influence of these uncertainties only grows if we extrapolate our data over longer timescales.

We can calculate a long-term (i.e., multi-year) estimate of CO_2 emissions from Bagana by combining our campaign CO_2/SO_2 (mass ratio of 1.1 ± 0.1) with our mean ($\pm$standard deviation) SO_2 flux from TROPOMI observations in 2018–2022 (175 ± 234 td^{-1}). The resulting value of CO_2 flux, 193 ± 257 td^{-1}, and our campaign-only value of 320 ± 84 td^{-1}, are significantly lower than the value of $6,245 \pm 2,335$ td^{-1} predicted by Aiuppa et al. (2019), who placed Bagana as Earth's fifth ranked volcanic carbon source. The CO_2/SO_2 ratio (2.4 ± 0.7, predicted as described above) and the SO_2 flux (1,032–1,971 kt yr^{-1}, from satellite observations in 2005–2015 presented by Carn et al. (2017)) used by Aiuppa et al. (2019) in their computation of CO_2 flux are significantly higher than the values we measured in September 2019. Thus, our derived CO_2 emission rate is substantially lower and, in September 2019 at least, Bagana is unlikely to have been a significant contributor to global volcanic carbon emissions. During intervals of elevated activity, however, Bagana may indeed be one of the Earth's most important volcanic carbon emitters. Fresh magmas fed into the shallow reservoirs from depth are likely to release relatively carbon-rich gas (with CO_2/SO_2 perhaps comparable to Aiuppa et al. (2019)'s predicted value of 2.4 ± 0.7). We know that co-eruptive SO_2 fluxes at Bagana can exceed 10^4 td^{-1} (this study, McCormick Kilbride et al., 2019, and references therein). Thus, peak CO_2 emissions at Bagana may be up to two orders of magnitude greater than what we measured in September 2019.

The foregoing discussion exemplifies a major challenge: how to accurately quantify global volcanic emissions when individual volcanoes have emissions that vary widely through time. Recent attempts to quantify global volcanic sulfur (Carn et al., 2017) and carbon emissions (Aiuppa et al., 2019; Fischer et al., 2019; Werner

et al., 2019) partly agree with earlier studies (e.g., Andres & Kasgnoc, 1998) that certain volcanoes tend to rank highly from year to year and decade to decade. However, many other volcanoes once considered globally important sources of volatiles into the atmosphere are now exhibiting reduced activity and more modest emissions. Miyakejima, in the northern Izu-Bonin arc, was among the world's major SO_2 emitters following its effusive eruption in 2000 before an exponential drop in outgassing through the following decade (Carn et al., 2017; Kazahaya et al., 2004; Mori et al., 2013). Anatahan, in the Mariana arc, likewise retains a high ranking in global emissions inventories (Aiuppa et al., 2019; Carn et al., 2017), notwithstanding the fact that ~85% of its SO_2 flux over the past three decades coincided with short-lived, intense eruptions, mostly in January–August 2005 (McCormick et al., 2015). Kilauea volcano on Hawaii has been a prodigious source of gas into the atmosphere for decades, yet following the end of the 2018 East Rift Zone eruption, SO_2 emissions fell below 100 td^{-1} (Elias et al., 2018; Kern et al., 2020). Conversely, Turrialba volcano in Costa Rica, awakened from a lengthy repose in 2018 and now dominates SO_2 and CO_2 emissions in the Central American Volcanic Arc (de Moor et al., 2017, cf. Mather et al., 2006, and references therein). These data, and the picture of Bagana we present herein, illustrate that highly variable gas emission rates (and potentially composition, too) are inherent to many volcanoes and this fact could, and should, be better incorporated into volcanic emissions inventories.

Quantifying the temporal variability of volcanic emissions over longer timeframes is essential if we are to fully evaluate the influence of volcanic outgassing to the composition of Earth's atmosphere and consequently to planetary climate. The period of observations at volcanoes is still relatively short compared to the cycles of activity (Werner et al., 2019). Short duration campaign data sets will seldom fully characterize highly dynamic systems and it follows that many volcanoes worldwide are inadequately characterized in terms of their outgassing flux and that many of our measurements are biased because they are often made during the most active periods (Werner et al., 2019). Long-term, more sustained and integrated emissions monitoring is required, melding synoptic satellite observations, automated ground-based remote sensing, permanently installed MultiGAS stations, regular sampling and analysis of emitted gases, and a key role for UAS in acquiring measurements and samples from otherwise inaccessible gas plumes (Edmonds, 2021; James et al., 2020; Kern et al., 2022).

4.2. Aerial Strategies for Volcano Monitoring

Our UAS gas sensing flights enabled the first measurements of gas composition and CO_2 outgassing from Bagana's otherwise inaccessible summit. The great potential of UAS in volcanic gas monitoring and research is evident (James et al., 2020; Liu, Aiuppa, et al., 2020; Pering et al., 2020; Shinohara et al., 2020; Stix et al., 2018). In particular, flying beyond visual line of sight (BVLOS) enables safe access to volcanic plumes from a distance of several kilometres, removing the need to climb unstable edifices to access summit vents directly (Liu, Aiuppa, et al., 2020; Schellenberg et al., 2019; Wood et al., 2020).

This study demonstrates that airborne MultiGAS measurements can recover volcanic plume gas composition robustly but challenges do remain. Our MultiGAS data sets are of shorter duration than ground-based studies, where the instrument may be exposed to gas for several days or installed permanently (e.g., Aiuppa et al., 2007; de Moor et al., 2016). Our instruments encountered relatively low gas concentrations over Bagana (cf. our experience of a more "open vent" system at Manam, Liu, Aiuppa, et al., 2020) but this is an inherent feature of airborne sampling versus ground-based MultiGAS deployments (Fischer & Lopez, 2016; Werner et al., 2013). Multi-rotor aircraft, which can hover in place, may enable more sustained plume exposure; however, multi-kilometer horizontal flight or ascent/descent with a multi-rotor is costly in terms of battery power, and the addition of more batteries greatly increases takeoff weight. The Titan cruises at roughly 20 ms^{-1} which allowed us to reach the volcanic summit plume quickly and gliding back toward the landing site allowed us to expend more battery power over the summit, thus increasing plume exposure times. Thermal energy in buoyant volcanic plumes may help to extend endurance further by reducing power consumption during summit traverses (Wood et al., 2020). In future, vertical take-off and landing (VTOL) aircraft may offer a combination of the fixed-wing flight into a volcanic plume from a distance of several kilometres, accompanied by a relatively prolonged gas-sensing interval hovering in the plume. For now, potential uncertainties in gas composition arising from short sensor exposure to the volcanic gas can be overcome, as here, by repeated flights and by manual traverses within each flight to maximize gas contact. Through our three successful flights, increasing time spent in the plume did demonstrably lead to decreased uncertainty on our recovered CO_2/SO_2 ratio (Figures 5b and 5d), although we cannot rule out that differences in the absolute value of the ratio from each flight are the result of spatial or temporal variations in gas composition.

Recovering UAS from distant and potentially turbulent airspace is no small feat, with changing volcanic activity potentially resulting in aircraft loss (Wood et al., 2020). Our work on Bagana directly followed our previous work on Manam and allowed us to explore our UAS capability further. One challenge we experienced was a telemetry shadow when the volcanic edifice lay between our ground station and the aircraft. We modified the geometry of our flight plans to minimize the time that the Titan spent in this radio "dead zone." We also flew closer to the volcanic summit than we had on Manam, at one point passing within 50 m altitude of the summit in pursuit of elevated gas concentrations. To achieve such close passes without aircraft loss requires high resolution and up-to-date topographic models for flight planning, which can be challenging to obtain for volcanoes with summit lava domes where active extrusion can modify topography by tens of meters. Moreover, a skilled pilot must monitor the in-flight FPV feed and take manual control in the event of turbulence or other threats to the aircraft. A full review of design requirements for successful fixed-wing UAS deployments is provided by Wood et al. (2020), resulting from volcanological fieldwork in recent years (Schellenberg et al., 2019; Liu, Aiuppa, et al., 2020; this study).

4.3. Future Volcano Monitoring at Bagana

Bagana is a remote volcano with no instrumented ground-based monitoring. A local observer provides regular radio reports of activity to Rabaul Volcanological Observatory (RVO) and community leaders liaise with the Bougainville Disaster Office (BDO) to discuss hazard mitigation and disaster risk reduction. The typical eruptive activity at Bagana, sluggish lava flows that are generally restricted to the cone, pose little direct hazard to populations in the surrounding villages (Figure 2). Of more concern are rare explosive eruptions which deposit hot ash on buildings, leading to fires and, more commonly, debris avalanches from the edifice into the upper reaches of the Torokina river.

In the absence of monitoring instruments, the main mitigation measures at Bagana are visits by RVO and BDO personnel to raise awareness among local communities of volcanic hazards. From our experience in the Wakovi and Piva communities, the level of hazard awareness is high among local people, with significant inter-generational memory of a range of activity styles. Moreover, a number of people described to us precursory phenomena they associate with imminent eruptions. This knowledge is among several factors influencing these communities' resilience: strong kinship relations with adjacent communities ensure alternative dwelling places may be sought in times of elevated activity, and families can mobilize and evacuate quickly. The major caveat to this perspective is how the level of risk (and capacity for mitigation) might vary in more unusual activity, for example, the rare high intensity explosive eruptions accompanied by pyroclastic flows known from Bagana's eruptive history (Bultitude et al., 1978). It remains unknown why these events occur. Possibilities include mafic recharge introducing volatile-rich magma into the shallow plumbing system (e.g., Roberge et al., 2009), changes in the supply of gas from deeper reservoirs into the shallow plumbing system (e.g., Edmonds et al., 2022; Liu, Cashman, et al., 2020), or hydrothermal mineralization sealing fractures in the summit dome and generating overpressure in the slowly degassing magma beneath (e.g., Heap et al., 2021). The scarcity of these events and therefore the limited experience of local communities in witnessing characteristic precursory behavior increases community vulnerability. In our discussions with Wakovi residents, a recurring suggestion we heard was that the absence of a strong visible gas plume from Bagana's summit would be perceived unusual or uncharacteristic and potentially taken as evidence of an imminent eruption; this was usually illustrated via the analogy of a steaming cooking pot with a closely fitting lid.

The BVLOS measurements we describe herein require a skilled pilot and access to electronic components, so are not, in our judgment, yet feasible for regular monitoring in isolated locations such as the interior of Bougainville. Less complex UAS operations, such as deploying commercially available multi-rotor aircraft with onboard cameras for observations of changing unrest or edifice stability (e.g., accumulation of avalanche material on upper slopes) might be more feasible. Regular UAS-based surveillance and measurements of volcanic emissions have been recently adopted by RVO at other volcanoes, notably gas sensing flights at Rabaul and observations of the evolving lava flow hazard during the 2019 Ulawun flank fissure eruption. For now, a more realistic monitoring strategy for remote volcanoes in PNG may be the provision of satellite data to RVO, in near-real-time, that could be relayed to BDO or even communities in the Torokina region for dissemination to the surrounding villages. Such a strategy faces its own challenges, in terms of resourcing the regular analysis of satellite observations, timely and accurate transmission to RVO, data storage and processing capacity at the observatory, and

reliable radio transmission to the remote interior of Bougainville. These challenges are set within a complex geopolitical context, with regional and national governments presently engaged in negotiations over the potential secession of Bougainville from Papua New Guinea. The foregoing discussion serves to illustrate the numerous challenges facing monitoring of remote volcanoes, particularly those capable of sustained eruptive activity, and also to emphasize the important and sometimes underappreciated role of local resilience measures in safeguarding populations from volcanic hazards.

5. Conclusions

We used UAS to fly a custom-built MultiGAS instrument into the summit plume of Bagana, a remote and persistently active volcano, and achieved the first measurements of the composition of Bagana gas emissions. We have demonstrated, building on our previous work, that fixed-wing UAS operating beyond visual line of sight are a powerful tool to study emissions from otherwise inaccessible vents. The short residence times we achieved in the plume (e.g., relative to conventional ground-based MultiGAS deployments) can be compensated for by repeated flights intercepting the plume. The uncertainties on our obtained plume composition data diminish with increased plume exposure, but such integration limits our ability to reconstruct temporal or spatial variations in gas composition. In future work, we aim to overcome these challenges, for example, by developing an aircraft that can hover or otherwise maintain prolonged contact between the gas sensor payload and the volcanic plume.

By combining our plume composition data with coincident remote sensing measurements of SO_2 emissions, we have derived a first estimate of CO_2 flux from Bagana, widely considered to be among Earth's major "known unknown" sources of deep carbon into the atmosphere. Our fieldwork coincided with an interval of low-level activity at Bagana and our CO_2 emission rates were, accordingly, substantially lower than anticipated (200–320 td^{-1} based on our data, vs. a predicted flux of 6,200 td^{-1} by Aiuppa et al. (2019)). Using multi-year satellite data, we have shown that Bagana's activity, like many volcanoes, is subject to wide temporal variations, and consequently outgassing rates vary widely too. Without any knowledge of the time dependence of plume composition (i.e., CO_2/SO_2), we argue that it is incorrect to extrapolate our short campaign data into longer term emissions estimates. In September 2019, Bagana was not likely to be among the major global volcanic carbon emitters. During intervals of elevated unrest, when both CO_2/SO_2 ratio and SO_2 emissions are likely to be higher than our measurements, we might anticipate CO_2 emission rates of $>10^4$ td^{-1}. A major challenge for the global volcanological research and monitoring community is how to capture variable gas composition at remote volcanoes or those otherwise without continuous or repeated measurements of gas chemistry. In the immediate term, long-term monitoring of such remote volcanoes as Bagana is likely to depend heavily on satellite observations, for example, the SO_2 and thermal data we present here, with regular deployments of UAS potentially being made by local and regional observatory staff during periods of heightened unrest and threat.

Data Availability Statement

Our data are stored in the Earthchem repository, specifically the DECADE portal, which has recently been developed for the archival of volcanic gas data, including time series (https://earthchem.org/ecl/). The data are archived at McCormick et al. (2023): https://doi.org/10.26022/IEDA/112898.

References

Aiuppa, A., Federico, C., Giudice, G., & Gurrieri, S. (2005). Chemical mapping of a fumarolic field: La Fossa crater, Vulcano Island (Aeolian Islands, Italy). *Geophysical Research Letters*, *32*(13), 1–4. https://doi.org/10.1029/2005GL023207

Aiuppa, A., Fischer, T. P., Plank, T., & Bani, P. (2019). CO_2 flux emissions from the Earth's most actively degassing volcanoes, 2005–2015. *Scientific Reports*, *9*(1), 5442. https://doi.org/10.1038/s41598-019-41901-y

Aiuppa, A., Moretti, R., Federico, C., Giudice, G., Gurrieri, S., Liuzzo, M., et al. (2007). Forecasting Etna eruptions by real-time observation of volcanic gas composition. *Geology*, *35*(12), 1115–1118. https://doi.org/10.1130/g24149a.1

Andres, R. J., & Kasgnoc, A. D. (1998). A time-averaged inventory of subaerial volcanic sulfur emissions. *Journal of Geophysical Research*, *103*(D19), 25251–25261. https://doi.org/10.1029/98jd02091

Blake, D. H. (1968). Post Miocene volcanoes on Bougainville Island, territory of Papua and New Guinea. *Bulletin Volcanologique*, *32*(1), 121–138. https://doi.org/10.1007/bf02596588

Bultitude, R. (1976). Eruptive history of Bagana volcano, Papua New Guinea, between 1882 and 1975. In R. Johnson (Ed.), *Volcanism in Australasia* (pp. 317–336). Elsevier.

Bultitude, R., Johnson, R., & Chappell, B. (1978). Andesites of Bagana volcano, Papua New Guinea: Chemical stratigraphy, and a reference andesite composition. *BMR Journal of Australian Geology and Geophysics*, *3*, 281–295.

Bultitude, R. J. (1981). Literature search for pre-1945 sightings of volcanoes and their activity on Bougainville Island. *Cooke-Ravian volume of volcanological papers* (pp. 227–242).

Bultitude, R. J., & Cooke, R. J. S. (1981). Note on activity from Bagana volcano from 1975 to 1980. *Cooke-Ravian volume of volcanological papers* (pp. 243–248).

Burton, M., Hayer, C., Miller, C., & Christenson, B. (2021). Insights into the 9 December 2019 eruption of Whakaari/White Island from analysis of TROPOMI SO_2 imagery. *Science Advances*, *7*(25), eabg1218. https://doi.org/10.1126/sciadv.abg1218

Campion, R., Delgado-Granados, H., & Mori, T. (2015). Image-based correction of the light dilution effect for SO_2 camera measurements. *Journal of Volcanology and Geothermal Research*, *300*, 48–57. https://doi.org/10.1016/j.jvolgeores.2015.01.004

Carn, S. A., Fioletov, V. E., Mclinden, C. A., Li, C., & Krotkov, N. A. (2017). A decade of global volcanic SO_2 emissions measured from space. *Scientific Reports*, *7*(1), 44095. https://doi.org/10.1038/srep44095

Coppola, D., Laiolo, M., Cigolini, C., Delle Donne, D., & Ripepe, M. (2016). Enhanced volcanic hot-spot detection using MODIS IR data: Results from the MIROVA system. *Geological Society Special Publication*, *426*(1), 181–205. https://doi.org/10.1144/sp426.5

Coppola, D., Laiolo, M., Cigolini, C., Massimetti, F., Delle Donne, D., Ripepe, M., et al. (2020). Thermal remote sensing for global volcano monitoring: Experiences from the MIROVA system. *Frontiers of Earth Science*, *7*, 362. https://doi.org/10.3389/feart.2019.00362

Crook, K. A. W. (1987). Petrology and mineral chemistry of sedimentary rocks from the Western Solomon Sea. *Geo-Marine Letters*, *6*(4), 203–209. https://doi.org/10.1007/bf02239581

D'Aleo, R., McCormick, B., Salem, L., Edmonds, M., Bitetto, M., Tamburello, G., et al. (2017). Preliminary results of a multi-parametric characterization of gas manifestations from volcanoes in west Papua New Guinea. In *Conferenza Rittmann Giovani Ricercatori*.

de Moor, J. M., Aiuppa, A., Avard, G., Wehrmann, H., Dunbar, N., Muller, C., et al. (2016). Turmoil at Turrialba Volcano (Costa Rica): Degassing and eruptive processes inferred from high-frequency gas monitoring. *Journal of Geophysical Research: Solid Earth*, *121*(8), 5761–5775. https://doi.org/10.1002/2016jb013150

de Moor, J. M., Kern, C., Avard, G., Muller, C., Aiuppa, A., Saballos, A., et al. (2017). A new sulfur and carbon degassing inventory for the Southern Central American Volcanic Arc: The importance of accurate time-series data sets and possible tectonic processes responsible for temporal variations in arc-scale volatile emissions. *Geochemistry, Geophysics, Geosystems*, *18*(12), 4437–4468. https://doi.org/10.1002/2017gc007141

Draxler, R. R., & Hess, G. D. (1998). An overview of the HYSPLIT_4 modeling system of trajectories, dispersion, and deposition. *Australian Meteorological Magazine*, *47*, 295–308.

Edmonds, M. (2021). Geochemical monitoring of volcanoes and the mitigation of volcanic gas hazards. In P. Papale (Ed.), *Forecasting and planning for volcanic hazards, risks, and disasters*. Elsevier.

Edmonds, M., Liu, E. J., & Cashman, K. V. (2022). Open-vent volcanoes fuelled by depth-integrated magma degassing. *Bulletin of Volcanology*, *84*(3), 28. https://doi.org/10.1007/s00445-021-01522-8

Elias, T., Kern, C., Horton, K. A., Sutton, A. J., & Garbeil, H. (2018). Measuring SO_2 emission rates at Kīlauea Volcano, Hawaii, using an array of upward-looking UV spectrometers, 2014–2017. *Frontiers of Earth Science*, *214*. https://doi.org/10.3389/feart.2018.00214

Fischer, T. P., Arellano, S., Carn, S., Aiuppa, A., Galle, B., Allard, P., et al. (2019). The emissions of CO_2 and other volatiles from the world's subaerial volcanoes. *Scientific Reports*, *9*(1), 18716. https://doi.org/10.1038/s41598-019-54682-1

Fischer, T. P., & Lopez, T. M. (2016). First airborne samples of a volcanic plume for $\delta^{13}C$ of CO_2 determinations. *Geophysical Research Letters*, *43*(7), 3272–3279. https://doi.org/10.1002/2016gl068499

Galle, B., Oppenheimer, C., Geyer, A., McGonigle, A. J. S., Edmonds, M., & Horrocks, L. (2003). A miniaturised ultraviolet spectrometer for remote sensing of SO_2 fluxes: A new tool for volcano surveillance. *Journal of Volcanology and Geothermal Research*, *119*(1–4), 241–254. https://doi.org/10.1016/s0377-0273(02)00356-6

Gliß, J., Stebel, K., Kylling, A., Dinger, A. S., Sihler, H., & Sudbø, A. (2017). *Pyplis*—A python software toolbox for the analysis of SO_2 camera images for emission rate retrievals from point sources. *Geosciences*, *7*(4), 134. https://doi.org/10.3390/geosciences7040134

Global Volcanism Program. (1983). Report on Bagana (Papua New Guinea). In L. McClelland (Ed.), *Scientific event alert network bulletin* (Vol. 8, p. 9). Smithsonian Institution. https://doi.org/10.5479/si.GVP.SEAN198309-255020

Global Volcanism Program. (1989). Report on Bagana (Papua New Guinea). In L. McClelland (Ed.), *Scientific event alert network bulletin* (Vol. 14, p. 7). Smithsonian Institution. https://doi.org/10.5479/si.GVP.SEAN198907-255020

Global Volcanism Program. (2019a). Report on Bagana (Papua New Guinea). In E. Venzke (Ed.), *Bulletin of the global volcanism network* (Vol. 50, p. 1). Smithsonian Institution. https://doi.org/10.5479/si.GVP.BGVN201902-255020

Global Volcanism Program. (2019b). Report on Bagana (Papua New Guinea). In A. E. Crafford & E. Venzke (Eds.), *Bulletin of the global volcanism network* (Vol. 44, p. 6). Smithsonian Institution. https://doi.org/10.5479/si.GVP.BGVN201906-25502

Global Volcanism Program. (2019c). Report on Bagana (Papua New Guinea). In K. L. Bennis, & E. Venzke (Eds.), *Bulletin of the global volcanism network* (Vol. 44, p. 12). Smithsonian Institution. https://doi.org/10.5479/si.GVP.BGVN201912-255020

Global Volcanism Program. (2020). Report on Bagana (Papua New Guinea). In E. Venzke (Ed.), *Bulletin of the global volcanism network* (Vol. 45, p. 7). Smithsonian Institution. https://doi.org/10.5479/si.GVP.BGVN202007-255020

Global Volcanism Program. (2021a). Report on Bagana (Papua New Guinea). In K. L. Bennis & E. Venzke (Eds.), *Bulletin of the global volcanism network* (Vol. 46, p. 1). Smithsonian Institution. https://doi.org/10.5479/si.GVP.BGVN202101-255020

Global Volcanism Program. (2021b). Report on Bagana (Papua New Guinea). In K. L. Bennis, & E. Venzke (Eds.), *Bulletin of the global volcanism network* (Vol. 46, p. 9). Smithsonian Institution.

Heap, M. J., Baumann, T., Gilg, H. A., Kolzenburg, S., Ryan, A. G., Villeneuve, M., et al. (2021). Hydrothermal alteration can result in pore pressurization and volcano instability. *Geology*, *49*(11), 1348–1352. https://doi.org/10.1130/g49063.1

Hergt, J., Woodhead, J., & Johnson, R. W. (2018). Potassium enrichment in arc lavas: A case study from Bougainville Island. In *State of the arc conference 2018*.

Holm, R. J., Rosenbaum, G., & Richards, S. W. (2016). Post 8 Ma reconstruction of Papua New Guinea and Solomon Islands: Microplate tectonics in a convergent plate boundary setting. *Earth-Science Reviews*, *156*, 66–81. https://doi.org/10.1016/j.earscirev.2016.03.005

James, M. R., Carr, B. B., D'Arcy, F., Diefenbach, A. K., Dietterich, H. R., Fornaciai, A., et al. (2020). Volcanological applications of unoccupied aircraft systems (UAS): Developments, strategies, and future challenges. *Volcanica*, *3*(1), 64–114.

Kantzas, E. P., McGonigle, A. J. S., Tamburello, G., Aiuppa, A., & Bryant, R. G. (2010). Protocols for UV camera volcanic SO_2 measurements. *Journal of Volcanology and Geothermal Research*, *194*(1–3), 55–60. https://doi.org/10.1016/j.jvolgeores.2010.05.003

Kazahaya, K., Shinohara, H., Uto, K., Odai, M., Nakahori, Y., Mori, H., et al. (2004). Gigantic SO_2 emission from Miyakejima volcano, Japan, caused by caldera collapse. *Geology*, *32*(5), 425–428. https://doi.org/10.1130/g20399.1

Kazahaya, R., Shinohara, H., Ohminato, T., & Kaneko, T. (2019). Airborne measurements of volcanic gas composition during unrest at Kuchinoerabujima volcano, Japan. *Bulletin of Volcanology*, *81*(2), 7. https://doi.org/10.1007/s00445-018-1262-9

Kern, C., Aiuppa, A., & de Moor, J. M. (2022). A golden era for volcanic gas geochemistry? *Bulletin of Volcanology*, *84*(5), 43. https://doi.org/10.1007/s00445-022-01556-6

Kern, C., Deutschmann, T., Werner, C., Sutton, A. J., Elias, T., & Kelly, P. J. (2012). Improving the accuracy of SO_2 column densities and emission rates obtained from upward-looking UV-spectroscopic measurements of volcanic plumes by taking realistic radiative transfer into account. *Journal of Geophysical Research*, *117*(20), D20302. https://doi.org/10.1029/2012jd017936

Kern, C., Kick, F., Lübcke, P., Vogel, L., Wöhrbach, M., & Platt, U. (2010). Theoretical description of functionality, applications, and limitations of SO_2 cameras for the remote sensing of volcanic plumes. *Atmospheric Measurement Techniques Discussions*, *3*(1), 531–578.

Kern, C., Lerner, A. H., Elias, T., Nadeau, P. A., Holland, L., Kelly, P. J., et al. (2020). Quantifying gas emissions associated with the 2018 rift eruption of Kīlauea Volcano using ground-based DOAS measurements. *Bulletin of Volcanology*, *82*(7), 55. https://doi.org/10.1007/s00445-020-01390-8

Liu, E. J., Aiuppa, A., Alan, A., Arellano, S., Bitetto, M., Bobrowski, N., et al. (2020). Aerial strategies advance volcanic gas measurements at inaccessible, strongly degassing volcanoes. *Science Advances*, *6*(44), abb9103. https://doi.org/10.1126/sciadv.abb9103

Liu, E. J., Cashman, K. V., Miller, E., Moore, H., Edmonds, M., Kunz, B. E., et al. (2020). Petrologic monitoring at Volcán de Fuego, Guatemala. *Journal of Volcanology and Geothermal Research*, *405*, 107044. https://doi.org/10.1016/j.jvolgeores.2020.107044

Liu, E. J., Wood, K., Mason, E., Edmonds, M., Aiuppa, A., Giudice, G., et al. (2019). Dynamics of outgassing and plume transport revealed by proximal unmanned aerial system (UAS) measurements at Volcán Villarrica, Chile. *Geochemistry, Geophysics, Geosystems*, *20*(2), 730–750. https://doi.org/10.1029/2018gc007692

Massimetti, F., Coppola, D., Laiola, M., Valade, S., Cigolini, C., & Ripepe, M. (2020). Volcanic hot-spot detection using SENTINEL-2: A comparison with MODIS-MIROVA thermal data series. *Remote Sensing*, *12*(5), 820. https://doi.org/10.3390/rs12050820

Mather, T. A., Pyle, D. M., Tsanev, V. I., McGonigle, A. J. S., Oppenheimer, C., & Allen, A. G. (2006). A reassessment of current volcanic emissions from the Central American arc with specific examples from Nicaragua. *Journal of Volcanology and Geothermal Research*, *149*(3–4), 297–311. https://doi.org/10.1016/j.jvolgeores.2005.07.021

McCormick, B., Popp, C., Andrews, B., & Cottrell, E. (2015). Ten years of satellite observations reveal highly variable sulphur dioxide emissions at Anatahan Volcano, Mariana Islands. *Journal of Geophysical Research: Atmospheres*, *120*(14), 7258–7282. https://doi.org/10.1002/2014jd022856

McCormick, B. T., Edmonds, M., Mather, T. A., & Carn, S. A. (2012). First synoptic analysis of volcanic degassing in Papua New Guinea. *Geochemistry, Geophysics, Geosystems*, *13*(3), 7. https://doi.org/10.1029/2011gc003945

McCormick, B. T., Nicholson, E. J., Wood, K., Wilkes, T., Schipper, I., Mulina, K., et al. (2023). Temporal variability in gas emissions at Bagana Volcano revealed by aerial, ground, and satellite observations, (version 1.0) [Dataset]. Interdisciplinary Earth Data Alliance (IEDA). https://doi.org/10.26022/IEDA/112898

McCormick Kilbride, B. T., Mulina, K., Wadge, G., Johnson, R. W., Itikarai, I., & Edmonds, M. (2019). Multi-year satellite observations of sulfur dioxide gas emissions and lava extrusion at Bagana volcano, Papua New Guinea. *Frontiers of Earth Science*, *7*, 9. https://doi.org/10.3389/feart.2019.00009

McGonigle, A. J. S., Aiuppa, A., Giudice, G., Tamburello, G., Hodson, A. J., & Gurrieri, S. (2008). Unmanned aerial vehicle measurements of volcanic carbon dioxide fluxes. *Geophysical Research Letters*, *35*(6), L06303. https://doi.org/10.1029/2007gl032508

McGonigle, A. J. S., Oppenheimer, C., Tsanev, V. I., Saunders, S., Mulina, K., Tohui, S., et al. (2004). Sulphur dioxide fluxes from Papua New Guinea's volcanoes. *Geophysical Research Letters*, *31*(8), L086061–L086064. https://doi.org/10.1029/2004GL019568

Mori, T., & Burton, M. (2006). The SO_2 camera: A simple, fast and cheap method for ground-based imaging of SO_2 in volcanic plumes. *Geophysical Research Letters*, *33*(24), L24804. https://doi.org/10.1029/2006gl027916

Mori, T., Shinohara, H., Kazahaya, K., Hirabayashi, J.-I., Matsushima, T., Mori, T., et al. (2013). Time-averaged SO_2 fluxes of subduction-zone volcanoes: Example of a 32-year exhaustive survey for Japanese volcanoes. *Journal of Geophysical Research: Atmospheres*, *118*(15), 8662–8674. https://doi.org/10.1002/jgrd.50591

Pering, T. D., Liu, E. J., Wood, K., Wilkes, T. C., Aiuppa, A., Tamburello, G., et al. (2020). Combined ground and aerial measurements resolve vent-specific gas fluxes from a multi-vent volcano. *Nature Communications*, *11*(1), 3039. https://doi.org/10.1038/s41467-020-16862-w

Queißer, M., Burton, M., Theys, N., Pardini, F., Salerno, G., Caltabiano, T., et al. (2019). TROPOMI enables high resolution SO_2 flux observations from Mt. Etna, Italy, and beyond. *Scientific Reports*, *9*(1), 957. https://doi.org/10.1038/s41598-018-37807-w

Roberge, J., Delgado-Granados, H., & Wallace, P. J. (2009). Mafic magma recharge supplies high CO_2 and SO_2 gas fluxes from Popocatépetl volcano, Mexico. *Geology*, *37*(2), 107–110. https://doi.org/10.1130/g25242a.1

Rüdiger, J., Tirpitz, J.-L., Maarten De Moor, J., Bobrowski, N., Gutmann, A., Liuzzo, M., et al. (2018). Implementation of electrochemical, optical and denuder-based sensors and sampling techniques on UAV for volcanic gas measurements: Examples from Masaya, Turrialba and Stromboli volcanoes. *Atmospheric Measurement Techniques*, *11*(4), 2441–2457. https://doi.org/10.5194/amt-11-2441-2018

Schellenberg, B., Richardson, T., Watson, M., Greatwood, C., Clarke, R., Thomas, R., et al. (2019). Remote sensing and identification of volcanic plumes using fixed-wing UAVs over Volcán de Fuego, Guatemala. *Journal of Field Robotics*, *36*(7), 1192–1211. https://doi.org/10.1002/rob.21896

Shinohara, H., Kazahaya, R., Ohminato, T., Kaneko, T., Tsunogai, U., & Morita, M. (2020). Variation of volcanic gas composition at a poorly accessible volcano: Sakurajima, Japan. *Journal of Volcanology and Geothermal Research*, *407*, 107098. https://doi.org/10.1016/j.jvolgeores.2020.107098

Stix, J., de Moor, J. M., Rüdiger, J., Alan, A., Corrales, E., D'Arcy, F., et al. (2018). Using drones and miniaturized instrumentation to study degassing at Turrialba and Masaya Volcanoes, Central America. *Journal of Geophysical Research: Solid Earth*, *123*(8), 6501–6520. https://doi.org/10.1029/2018JB015655

Symonds, R. B., Gerlach, T. M., & Reed, M. H. (2001). Magmatic gas scrubbing: Implications for volcano monitoring. *Journal of Volcanology and Geothermal Research*, *108*(1–4), 303–341. https://doi.org/10.1016/s0377-0273(00)00292-4

Tamburello, G. (2015). Ratiocalc: Software for processing data from multicomponent volcanic gas analyzers. *Computers & Geosciences*, *82*, 63–67. https://doi.org/10.1016/j.cageo.2015.05.004

Theys, N., Fioletov, V., Li, C., De Smedt, I., Lerot, C., McLinden, C., et al. (2021). A sulfur dioxide covariance-based retrieval algorithm (COBRA): Application to TROPOMI reveals new emission sources. *Atmospheric Chemistry and Physics*, *21*(22), 16727–16744. https://doi.org/10.5194/acp-21-16727-2021

Theys, N., Hedelt, P., De Smedt, I., Lerot, C., Yu, H., Vlietinck, J., et al. (2019). Global monitoring of volcanic SO_2 degassing with unprecedented resolution from TROPOMI onboard Sentinel-5 Precursor. *Scientific Reports*, *9*(1), 2643. https://doi.org/10.1038/s41598-019-39279-y

Veefkind, J. P., Aben, I., McMullan, K., Förster, H., de Vries, J., Otter, G., et al. (2012). TROPOMI on the ESA Sentinel-5 Precursor: A GMES mission for global observations of the atmospheric composition for climate, air quality and ozone layer applications. *Remote Sensing of Environment*, *120*, 70–83. https://doi.org/10.1016/j.rse.2011.09.027

Wadge, G., McCormick Kilbride, B. T., Edmonds, M., & Johnson, R. W. (2018). Persistent growth of a young andesite lava cone: Bagana volcano, Papua New Guinea. *Journal of Volcanology and Geothermal Research*, *356*, 304–315. https://doi.org/10.1016/j.jvolgeores.2018.03.012

Wadge, G., Saunders, S., & Itikarai, I. (2012). Pulsatory andesite lava flow at Bagana Volcano. *Geochemistry, Geophysics, Geosystems*, *13*(11), Q11011. https://doi.org/10.1029/2012gc004336

Werner, C., Fischer, T., Aiuppa, A., Edmonds, M., Cardellini, C., Carn, S., et al. (2019). Carbon dioxide emissions from subaerial volcanic regions: Two decades in review. In B. Orcutt, I. Daniel, & R. Dasgupta (Eds.), *Deep carbon: Past to present*. Cambridge University Press.

Werner, C., Kelly, P. J., Doukas, M., Lopez, T., Pfeffer, M., McGimsey, R., & Neal, C. (2013). Degassing of CO_2, SO_2, and H_2S associated with the 2009 eruption of Redoubt Volcano, Alaska. *Journal of Volcanology and Geothermal Research*, *259*, 270–284. https://doi.org/10.1016/j.jvolgeores.2012.04.012

Wilkes, T. C., McGonigle, A. J. S., Pering, T. D., Taggart, A. J., White, B. S., Bryant, R. G., & Willmott, J. R. (2016). Ultraviolet imaging with low cost smartphone sensors: Development and application of a raspberry pi-based UV camera. *Sensors*, *16*(10), 1649. https://doi.org/10.3390/s16101649

Wilkes, T. C., Pering, T. D., McGonigle, A. J. S., Tamburello, G., & Willmott, J. R. (2017). A low-cost smartphone sensor-based UV camera for volcanic SO_2 emission measurements. *Remote Sensing*, *9*(1), 27. https://doi.org/10.3390/rs9010027

Wood, K., Liu, E. J., Aiuppa, A., GIudice, G., Bitetto, M., & Richardson, T. (2019). *A deconvolution-based sensor response correction for volcanic gas measurements, Poster F41*. Deep Carbon 2019.

Wood, K., Liu, E. J., Richardson, T., Clarke, R., Freer, J., Aiuppa, A., et al. (2020). BVLOS UAS operations in highly-turbulent volcanic plumes. *Frontiers in Robotics and AI*, *7*, 549716. https://doi.org/10.3389/frobt.2020.549716

Woodhead, J. D., Eggins, S. M., & Johnson, R. W. (1998). Magma genesis in the New Britain island arc: Further insights into melting and mass transfer processes. *Journal of Petrology*, *39*(9), 1641–1668. https://doi.org/10.1093/petroj/39.9.1641